

## Hadley Circulation as a Modulator of the Extratropical Climate

ARTHUR Y. HOU

*Data Assimilation Office, Laboratory for Atmospheres, NASA/Goddard Space Flight Center, Greenbelt, Maryland*

(Manuscript received 23 January 1996, in final form 15 October 1997)

### ABSTRACT

Studies based on GCM ensemble forecasts have shown that an intensification of the cross-equatorial Hadley circulation associated with a latitudinal displacement of the zonally averaged convective heating in the Tropics can lead to remote warming in the winter high latitudes. This work further investigates this tropical–extratropical connection in a perpetual winter experiment using an idealized GCM without orography to focus on the role of transient eddies, and tests against observations using a multiyear reanalysis produced by the Goddard Earth Observing System-Version 1 (GEOS-1) Data Assimilation System.

The GCM results show that the intensification and poleward expansion of the cross-equatorial Hadley cell induced by a tropical heating shift can lead to westerly acceleration in the winter subtropics and enhanced vertical shear of the zonal wind in the subtropics and midlatitudes. The increased baroclinicity outside the Tropics is accompanied by reduced meridional temperature and potential vorticity (PV) gradients, consistent with enhanced PV mixing and increased poleward heat transport by baroclinic eddies. But if the changes in the Hadley cell are such that they produce a deceleration of the zonal wind in the winter subtropics, stronger temperature and PV gradients result in the winter extratropics. The midlatitude response to Hadley acceleration of the subtropical jet is dominated by enhanced power in low-frequency planetary-scale waves that peaks at zonal wavenumber 2 with a period of 40 days.

The extent to which this tropical–extratropical connection may be present in nature is tested using the GEOS-1 reanalysis for five austral winters from 1985 to 1989. Results show that the year-to-year variation in the zonally averaged extratropical temperature gradient in austral winters is correlated with the variation in the acceleration of the subtropical zonal wind by the winter Hadley cell. The anomaly correlation coefficients range from 0.80 to 0.92, depending on the statistical test. The positive Hadley acceleration anomaly in the subtropics during the 1988 austral winter is accompanied by stronger than normal zonal wind shears in the subtropics and midlatitudes, a colder troposphere in the midlatitudes, and a warmer pole. The extratropical temperature anomalies are associated with a reduced PV gradient, and the midlatitude geopotential height anomaly shows a spectral peak at wavenumbers 2–3 with periods between 40 and 60 days, similar to the idealized GCM results. The implication of this study is that the Hadley circulation may play a role in modulating the temperature difference between middle and high latitudes by modifying the zonal wind shear in the subtropics and midlatitudes.

### 1. Introduction

Understanding the processes that regulate the pole-to-equator temperature difference is a central issue in climate dynamics (Lindzen 1994). In the Tropics, the rotationally confined, thermally direct Hadley circulations are important for maintaining the observed small meridional temperature gradients in low latitudes (Schneider 1977; Held and Hou 1980). Outside the Tropics, it has long been recognized that quasigeostrophic baroclinic eddies are responsible for transporting heat to the poles (Lorenz 1967). Since these are distinct physical mechanisms, dynamics of the Tropics and extratropics have often been analyzed in isolation from each other. Conceptually, these two dynamic re-

gimes may be coupled through the vertical shear of the zonal wind in the subtropics, whose strength depends on the rate of supply of angular momentum by the Hadley circulation and the mean-flow deceleration by extratropical eddies. It is plausible that a connection may exist between acceleration of the subtropical jet by the Hadley cell and the eddy-induced heat transport outside the Tropics.

Transport of heat by unstable baroclinic waves in the extratropics has been associated with synoptic-scale eddies along the midlatitude storm tracks, which can more readily sense the local zonal wind shear along the storm tracks than the subtropical jet (Hoskins and Valdes 1990). However, planetary-scale waves in the atmosphere can also be baroclinically unstable and play a role in determining the global climate, particularly if we consider the influence of meridional confinement by the subtropical jet (Ioannou and Lindzen 1986; Lindzen 1993). Studies have shown that significant contributions to global heat and vorticity fluxes come from planetary-

---

*Corresponding author address:* Dr. Arthur Y. Hou, Code 910.3, Laboratory for Atmospheres, NASA/Goddard Space Flight Center, Greenbelt, MD 20771.  
E-mail: arthur.hou@gsfc.nasa.gov

scale waves with periods longer than 10 days (e.g., Holopainen et al. 1982). Baroclinic activities along the storm tracks and the variability of storm tracks may also be modulated by low-frequency planetary waves and variations of the subtropical jetstream (e.g., Blackmon et al. 1977; Lau 1988; Nigam and Lindzen 1989). Given their global scales, planetary waves can be expected to be more effective than synoptic-scale eddies in modifying the zonally averaged climate. Any process that alters these low-frequency planetary waves can potentially be an effective modulator of the extratropical climate.

Studies of axisymmetric circulations have shown that the intensification of the Hadley cell associated with a small latitudinal shift or concentration of tropical heating can significantly alter the intensity of the subtropical jet in the absence of eddies (Lindzen and Hou 1988; Hou and Lindzen 1992). That the observed jet does not exhibit the same degree of sensitivity suggests that eddies must actively decelerate the jet in response to increased advection of angular momentum by the Hadley cell. The hypothesis that an intensified Hadley circulation can accelerate the subtropical jet in such a way as to increase the poleward heat transport in the winter extratropics was first tested in an ensemble forecast experiment by Hou (1993) using an idealized GCM with prescribed tropical heating and realistic orography. He showed that the intensification of a cross-equatorial Hadley cell induced by a shift of the tropical heating into the summer hemisphere led to statistically significant temperature anomalies in the winter extratropics due to increased poleward heat transport by low-frequency waves and wave-induced mean meridional circulation. Hou and Molod (1995) obtained similar results using the full GEOS GCM with detailed radiative flux calculations and parameterized moist physics. But the presence of orographically forced waves in these models complicated the interpretation of the role of transient eddies.

Chang (1995) recently used a simplified GCM without orography in a perpetual winter experiment to examine the extratropical response to an intensification of the winter Hadley cell induced by a concentrated tropical heating. He found that a stronger winter Hadley cell led to westerly acceleration in the Tropics, an equatorward shift of the zonal wind pattern, and warming in the midlatitude, but no meaningful signal in high latitudes. He interpreted the midlatitude warming in terms of an equatorward shift of the global heating pattern. This is seemingly incompatible with the original idea that a stronger Hadley cell can enhance baroclinic wave activity to increase heat transport to the winter high latitudes, which implies cooling in the midlatitudes and warming in the high latitudes [as in Hou and Molod (1995) and the enhanced low-frequency case in Hou (1993)]. The nature of the interaction between the Hadley cell and extratropical heat transport thus requires further investigation.

In this study we conduct a set of idealized GCM experiments to clarify some of these issues and test the hypothesis using a multiyear reanalysis produced by the GEOS-1 Data Assimilation System (Schubert et al. 1995). Specifically, we seek to clarify whether a stronger winter Hadley cell can accelerate the subtropical jet in such a way as to 1) increase the baroclinicity in the midlatitudes, 2) amplify transient eddy activities, and 3) reduce the zonal-mean temperature difference between the middle and high latitudes in the winter extratropics. The GCM experiments follow the basic methodology used in Hou (1993), except in a perpetual winter setting with no orography, as described in section 2. Sections 3 and 4 present results from the “off-equator heating” and “concentrated heating” experiments, respectively. The results from the GEOS-1 reanalysis are discussed in section 5, and the main conclusions are summarized in section 6.

## 2. Perpetual northern winter experiments

A series of 1000-day climate simulations were performed using a “dry” version of the Goddard Earth Observing System-Version 1 (GEOS-1) GCM (Takacs et al. 1994) in which radiation and moist convection modules were replaced by idealized functions and turbulent mixing was represented by a second-order vertical diffusion in the planetary boundary layer, as in Hou (1993). The model had no orography and was operated at a resolution of  $4^\circ$  lat  $\times$   $5^\circ$  long, and 20 sigma levels.

The diabatic forcing,  $Q$ , consists of a background heating simulating the equator-to-pole differential radiative driving from the surface,  $Q_{\text{rad}}$ , and a tropical convective heating,  $Q_c$ . The background heating was modeled by relaxing temperature,  $T$ , to a prescribed zonally symmetric, time-independent reference temperature,  $T_0(\phi, z)$ , where  $\phi$  is latitude and  $z$  is the log-pressure height; namely,  $Q_{\text{rad}} = -[T - T_0(\phi, z)]\tau^{-1}$ , where the relaxation time constant,  $\tau$ , is taken to be 20 days and  $T_0(\phi, z)$  is given in the appendix. The maximum of  $T_0$  was positioned at  $6^\circ\text{S}$  to simulate perpetual northern winter conditions in all experiments.

The prescribed tropical heating is zonally symmetric and steady in time and has the idealized structure for  $|\eta - \eta_c| \leq \pm\delta$ , and  $z \leq z_T$ :

$$Q_c(y, z) = Q_0 \sin\left(\frac{\pi z}{z_T}\right) \exp\left(-\frac{3z}{5H}\right) \cos^2\left(\frac{\pi(\eta - \eta_c)}{2\delta}\right),$$

where  $\eta$  is the sine of latitude,  $\eta_c$  defines the position of maximum heating,  $\delta$  is a “half-width” of 0.34 rad (about  $20^\circ$  lat),  $z_T$  is the top of convection set at 100 mb,  $H$  is a scale height taken to be 8 km, and  $Q_0 = 4.36 \times 10^{-5} \text{ K s}^{-1}$ , which yields a heating maximum of about  $2 \text{ K day}^{-1}$  at 450 mb.

The model was first integrated forward from a state of rest with  $Q_c$  on the equator for one year to provide

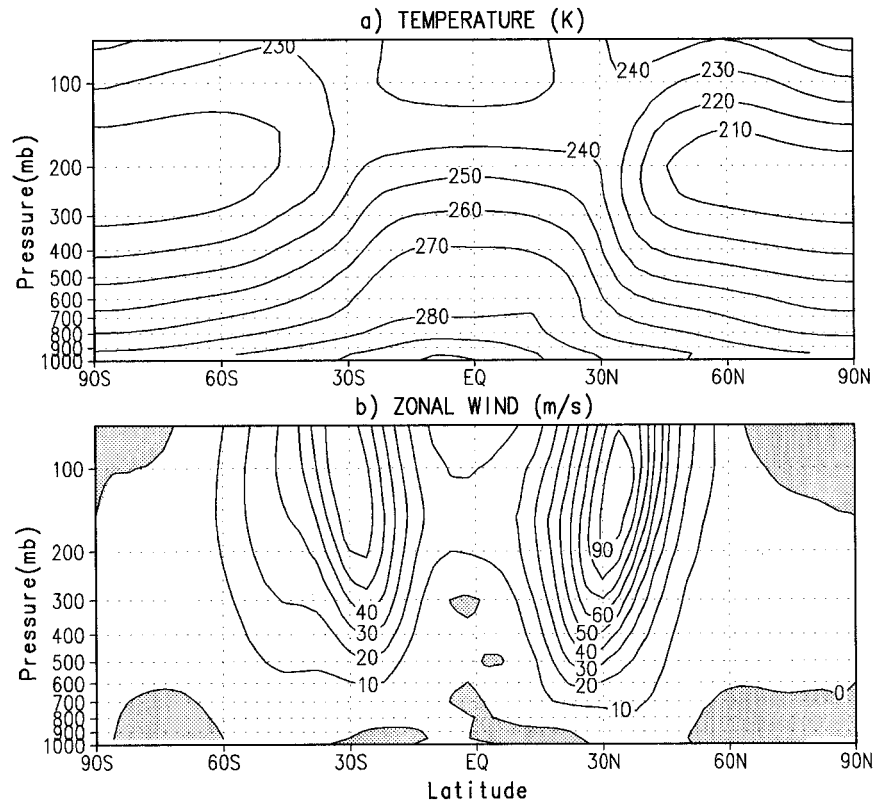


FIG. 1. Zonal-mean model climatology for the last 900 days of simulation with  $Q_c$  at  $6^\circ\text{S}$  (case B). (a) Temperature. (b) Zonal wind.

the initial condition for subsequent experiments. The integration was continued for another 1000 days with  $Q_c$  on the equator, to establish a “control” (case A). In the “off-equator heating” experiment (case B), the winter Hadley cell was intensified by centering  $Q_c$  at  $6^\circ\text{S}$  in a parallel 1000-day simulation. In a third simulation, the “narrow heating” experiment (case C), the integration was continued for another 1000 days from case B with the winter Hadley cell enhanced (relative to case B) by concentrating the tropical heating at  $6^\circ\text{S}$  while preserving the total  $Q_c$  (i.e.,  $\delta = 0.17$  rad and  $Q_0 = 8.72 \times 10^{-5} \text{ K s}^{-1}$ ). Note that  $Q_c$  never extended beyond  $26^\circ$  lat; poleward of  $26^\circ$  the prescribed forcing was identical in all three experiments so that temperature changes outside the Tropics may be considered as a “remote” response to the heating perturbation in the Tropics.

That the 1000-day simulation had reached a statistically steady state was verified by an approximate balance between the time-averaged diabatic and dynamic heating terms (with the tendency term at least two orders of magnitude smaller). Since the prescribed thermal forcing is zonally symmetric, the time-averaged fields must be zonally uniform without stationary wave forcing. For the last 900 days the time-mean eddy amplitudes relative to their zonal means were less than 0.15% temperature at 500 mb and 1.5% for zonal wind at 200 mb. The exception is the meridional wind whose zonal

mean is a small residual of the eddies but the eddy variance is effectively constant with time.

The time-averaged zonal-mean temperature and zonal wind for the last 900 days are shown in Fig. 1 for the off-equator heating case (case B), which is more in keeping with the observed precipitation climatology (Janowiak and Arkin 1991). Compared with observations, the zonally averaged subtropical jets in Fig. 1 are more intense, due in part to the absence of orography. The extent to which results based on a strongly baroclinic, idealized model may be applicable to the atmosphere is tested against observations in section 5.

### 3. Results for a stronger winter Hadley cell associated with a tropical heating displacement

In this section, the steady-state climate in case B (with  $Q_c$  at  $6^\circ\text{S}$ ) is compared with that in case A (with  $Q_c$  at the equator). Figure 2a shows that the heating perturbation associated with the  $6^\circ$  shift is confined to the Tropics, with a midtropospheric maximum of roughly  $0.9 \text{ K day}^{-1}$ . The intensification of the cross-equatorial “winter” Hadley cell is evident in the time-averaged meridional streamfunctions shown in Figs. 2b and 2c. Detailed wind and temperature adjustments within the Hadley cell domain (roughly  $30^\circ\text{S}$  to  $30^\circ\text{N}$ ) are discussed in section 3a.

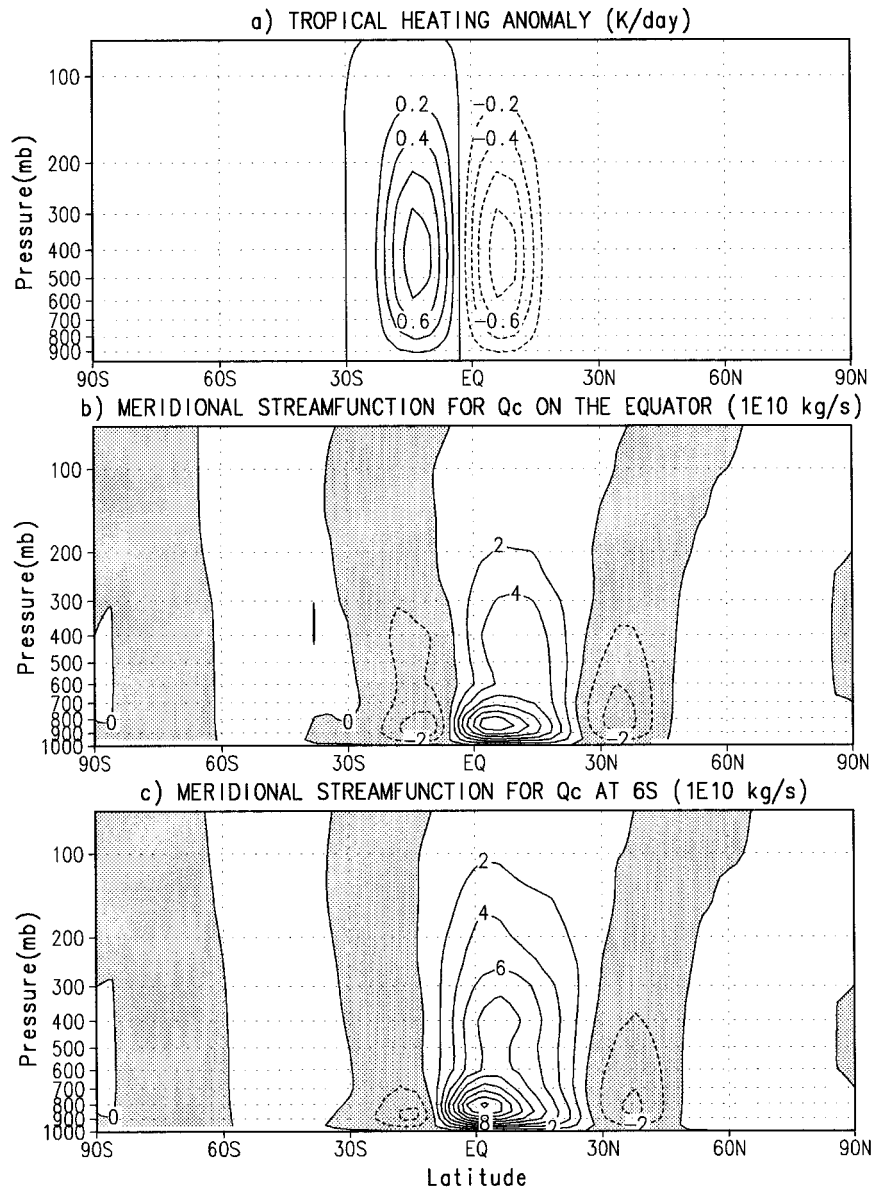


FIG. 2. (a) Anomaly associated with a  $6^\circ$  lat shift of the prescribed heating in the Tropics (case B minus case A). (b) Meridional streamfunction in units of  $10^{10} \text{ kg s}^{-1}$  averaged over the last 900 days case A. (c) Corresponding streamfunction in case B.

The time-averaged zonal-mean temperature anomaly (case B minus case A) and its statistical significance based on Student's *t*-test are shown in Fig. 3. The statistics were computed by dividing the 900-day time series into 45 samples of 20-day averages (similar results were obtained for 10- or 30-day sample sizes). This "remote response" in the winter extratropics to an intensification of the winter Hadley cell consists of mid-latitude cooling and high-latitude warming anomalies, similar to the ensemble forecast results of Hou (1993) and Hou and Molod (1995), except that in this perpetual winter simulation the anomalies are statistically more robust, particularly at the high latitudes. In a steady

state, diabatic heating must balance dynamic heating. In the extratropics where  $Q_c$  vanishes,  $Q_{\text{dyn}} = -Q_{\text{rad}} = (T - T_0)\tau^{-1}$ . Within this Newtonian cooling approximation, the temperature anomaly,  $\Delta T$ , is proportional to the dynamic heating anomaly; that is,  $\Delta T = (\Delta Q_{\text{dyn}})\tau$ . The winter extratropical temperature anomalies shown in Fig. 3 are therefore consistent with enhanced heat transport from the middle to high latitudes by eddies and the eddy-induced mean circulation.

A key assumption in this hypothesis is that a stronger Hadley cell can accelerate the subtropical jet in a way that enhances the baroclinicity from the subtropics to the midlatitudes, leading to increased poleward heat

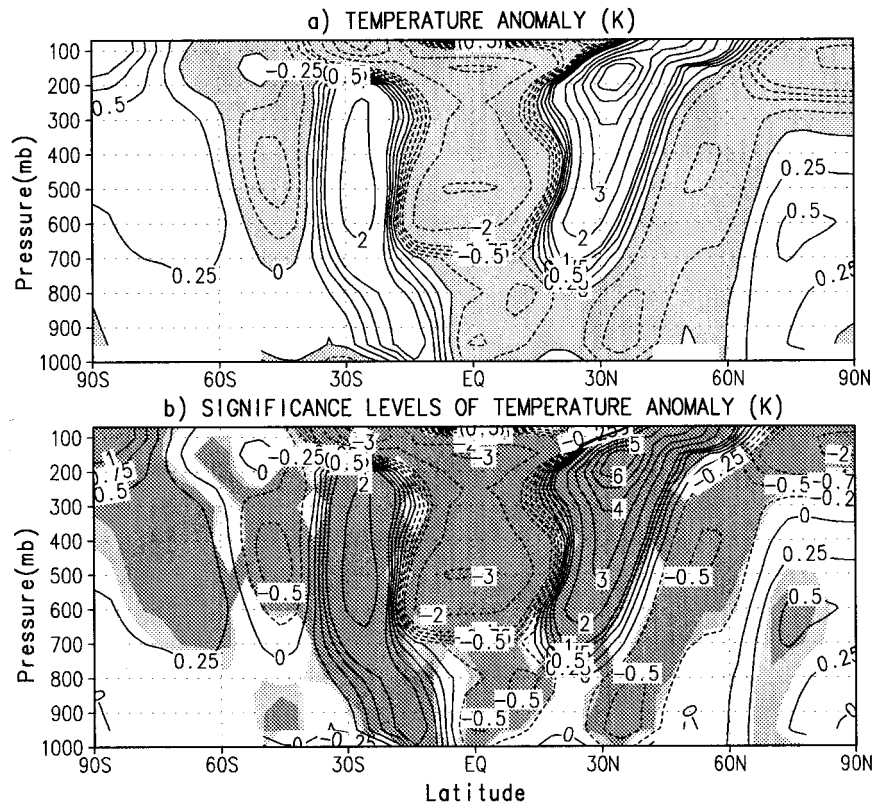


FIG. 3. (a) Time-averaged zonal-mean temperature anomaly for the last 900 days (case B minus case A). (b) Significance levels (shaded) of the anomaly (contours) given by Student's  $t$  test. Light-shade regions exceed 95% and dark-shade regions exceed 99%.

transport between the mid- and high latitudes. This enhanced baroclinicity is evident in the zonal wind anomaly shown in Fig. 4. Figure 5 shows that the meridional flux of absolute vorticity by the poleward branch of the Hadley cell (i.e., the “Hadley acceleration” above 300 mb between the equator and 30°N) increases with the Hadley cell intensity. The acceleration anomaly in this region should be differentiated from the positive anomaly along the poleward edge of the winter Hadley cell due to a weakened zonal deceleration by the mean meridional circulation (MMC) driven by the midlatitude eddies. The latter should be regarded as a part of the extratropical response to the intensification of the winter cell. One feature worth noting is that the positive wind and acceleration anomalies in the summer subtropics are associated with a poleward shift of the *equilibrium* position of a weak summer Hadley cell whose dynamic adjustment time is longer than a season. This is difficult to realize—except in a perpetual climate simulation, which would account for its absence in the forecast experiments by Hou (1993) and Hou and Molod (1995). In the remaining work we will focus on the winter Hadley cell and its interaction with the winter extratropics.

#### a. Adjustment of the zonal-mean climate within the Hadley cell domain

The temperature and zonal wind anomalies in the Tropics and subtropics in Figs. 3 and 4 may be understood in terms of an “equal area” Hadley cell model that conserves absolute angular momentum and potential temperature (Held and Hou 1980; Lindzen and Hou 1988). For the model parameters used in this study, the equal-area solutions for a Boussinesq Hadley cell with an assumed depth of 15 km are

$$\phi_0 = 4.69^\circ\text{S}, \quad \phi_s = 29.05^\circ\text{S}, \quad \phi_w = 32.66^\circ\text{N} \quad (\text{case A})$$

and

$$\phi_0 = 12.15^\circ\text{S}, \quad \phi_s = 30.80^\circ\text{S}, \quad \phi_w = 34.42^\circ\text{N}, \quad (\text{case B})$$

where  $\phi_s$  and  $\phi_w$  define the poleward boundaries of the summer and winter Hadley cells, respectively, and  $\phi_0$  is the boundary between the two cells. As the tropical heating is displaced to 6°S from the equator in case B, the northern winter Hadley cell is 25% wider and pen-

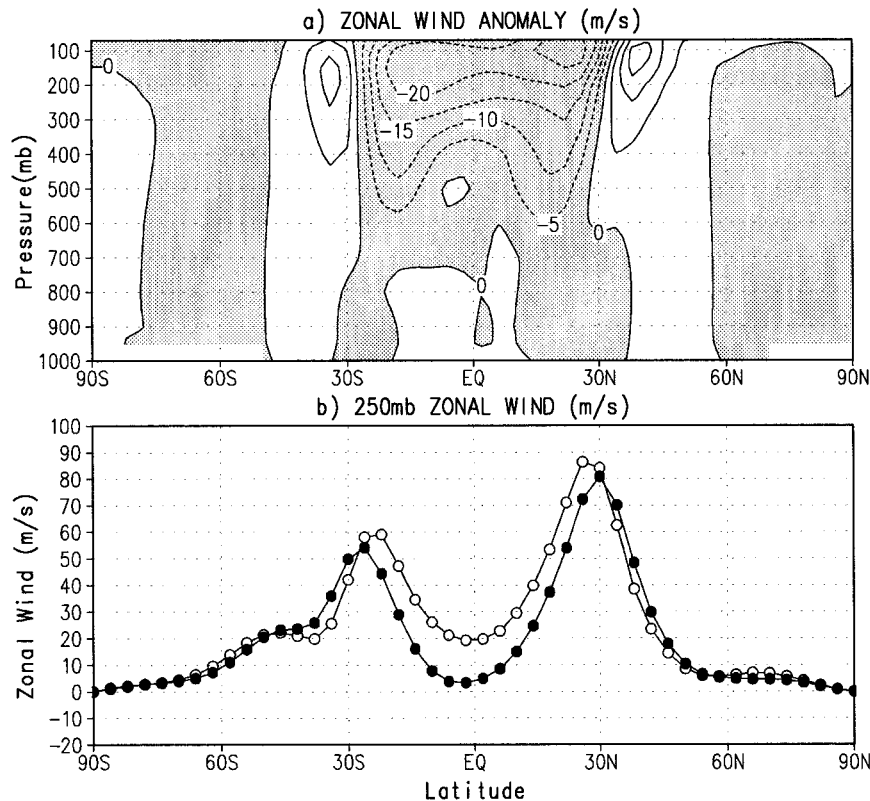


FIG. 4. (a) Time-averaged zonally averaged zonal wind anomaly for the last 900 days. (b) Corresponding zonal winds at 250 mb (open circles denote case A; solid circles denote case B).

etrates farther poleward, while the summer cell contracts but also extends farther poleward.

Figure 6a shows the equal-area solutions for the vertically averaged potential temperature and the prescribed “thermal equilibrium” potential temperatures (including the effect of  $Q_c$ ) for a state of no motion. The equal-area solution is obtained by requiring the area of diabatic warming equal that of cooling in a steady state. The departure of temperature from this equilibrium profile is proportional to the vertically averaged diabatic heating in balance with the averaged horizontal heat flux divergence (Held and Hou 1980).

Figure 6b shows that the time-averaged potential temperature anomaly at 500 mb from the GCM experiment is in good agreement with the vertically averaged anomaly predicted by the equal-area solution. Although the anomaly is roughly symmetric w.r.t. the equator, the adjustments leading to the warming anomalies in the subtropics are different in the two hemispheres. In the winter hemisphere, the tropical cooling and subtropical warming anomalies are due to the intensification and a northward expansion of the winter cell induced by a southward shift of the tropical heating (see the thermal-equilibrium temperature in Fig. 6a), while the subtropical warming in the summer hemisphere is associated with a contracted and weakened summer cell displaced

southward due to a southward shift of the tropical heating.

The zonal wind anomalies in Fig. 4 show an upper-level easterly bias within the Hadley cell domain, consistent with a maximum rising motion originating at a latitude farther away from the equator thus carrying less absolute angular momentum. Since the poleward boundaries of the equal-area Hadley cells coincide with the positions of the subtropical jets, the westerly wind biases in the subtropics are consistent with poleward movements of the Hadley cell boundaries predicted by the equal-area model. The upper-level westerly wind bias in Fig. 4 extends well into the winter midlatitudes and must therefore be at least partly controlled by eddies (see section 3c). Overall, eddies in this idealized GCM without orography do not appear to have altered the wind and temperature within the Hadley cell domain in a fundamental way from those predicted by the axisymmetric equal-area model.

#### b. Remote extratropical climate signals

Figure 7a shows that the winter extratropical temperature anomalies shown in Fig. 3 correspond to a reduced zonal-mean temperature difference between the winter middle and high latitudes. The reduction between

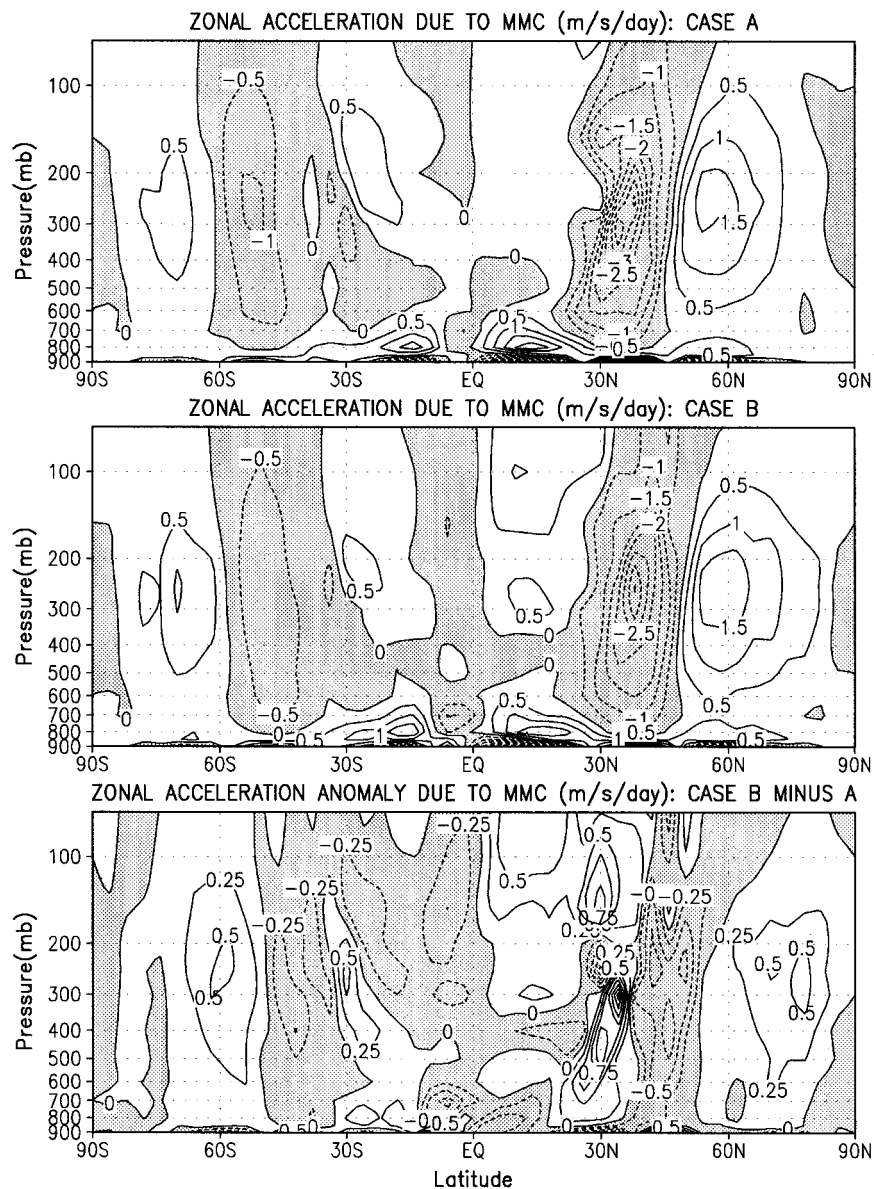


FIG. 5. Zonal acceleration due to the mean meridional circulation averaged over the last 900 days (the units are  $\text{m s}^{-1} \text{day}^{-1}$ ).

$45^{\circ}\text{N}$  and  $90^{\circ}\text{N}$  is about 1 K (out of 12 K) at 600 mb, with a vertically averaged reduction of about 0.8 K below 300 mb (Fig. 7b). Since the magnitude of this reduction depends partly on the static stability of the prescribed background  $T_0$ , which is somewhat larger than the observed in the winter extratropics (see appendix), the confinement of the high-latitude warming anomaly below 300 mb reflects the sharp increase in this background static stability above 300 mb. In terms of area-weighted temperature changes, the time-averaged midlatitude cold bias of  $-0.23$  K between  $40^{\circ}\text{N}$  and  $64^{\circ}\text{N}$  (Fig. 8a) and the warm bias of 0.31 K poleward of  $64^{\circ}\text{N}$  (Fig. 8b) represent a midlatitude cooling nearly twice the magnitude of the high-latitude warming, suggesting

that dynamic redistribution of heat may not account for all of the cooling in the midlatitudes.

The time series in Fig. 8 show that the time-averaged zonal-mean temperature anomalies in the winter extratropics are apparent residuals of low-frequency fluctuations, similar to the full GCM result shown in Hou and Molod (1995). That the reduction in the extratropical temperature difference was not established in the initial 50 days argues against it being a direct result of adjustment by synoptic-scale transients.

The space-time spectra of the transient eddies show that both the synoptic-scale and low-frequency waves in the winter extratropics are amplified by a stronger Hadley cell. In case A the midlatitude variance spectra

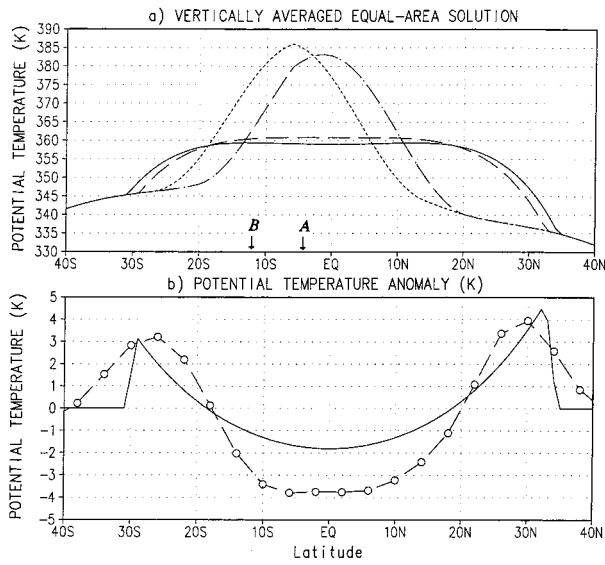


FIG. 6. (a) "Equal-area" solutions for the vertically averaged potential temperature (dashed for case A; solid for case B). Also shown are the prescribed thermal-equilibrium potential temperatures for case A (dash-dots) and case B (dots). The arrows labeled A and B mark the boundary between the winter and summer cells in cases A and B, respectively. (b) Comparison of the equal-area solution for the vertically averaged potential temperature anomaly (solid) with the potential temperature anomaly at 500 mb from GCM simulations (dashed).

of the transient meridional velocity  $v'$  at 500 mb (Fig. 9a) consist of dominant peaks at zonal wavenumber 5 with periods from 10 to 14 days, and secondary peaks at wavenumber 6 with a period of 9 days, and at wavenumbers 2 and 3 with periods of 40 and 18 days, re-

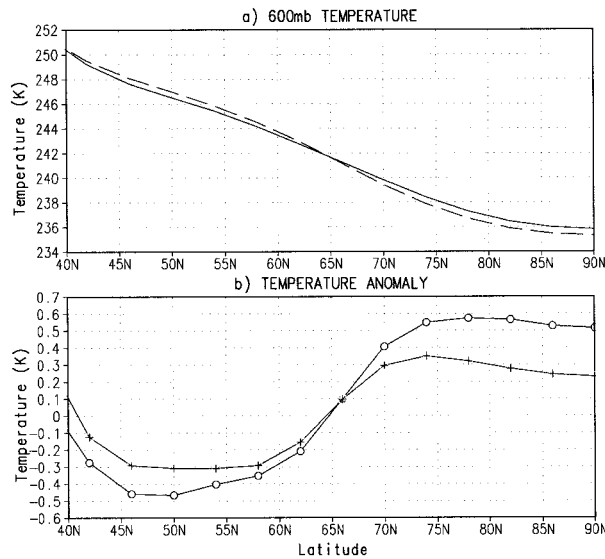


FIG. 7. (a) Time-averaged zonal-mean temperature profiles at 600 mb for case A (dashed) and case B (solid). (b) Corresponding temperature anomaly at 600 mb (open circles) and the averaged anomaly below 300 mb (plus signs).

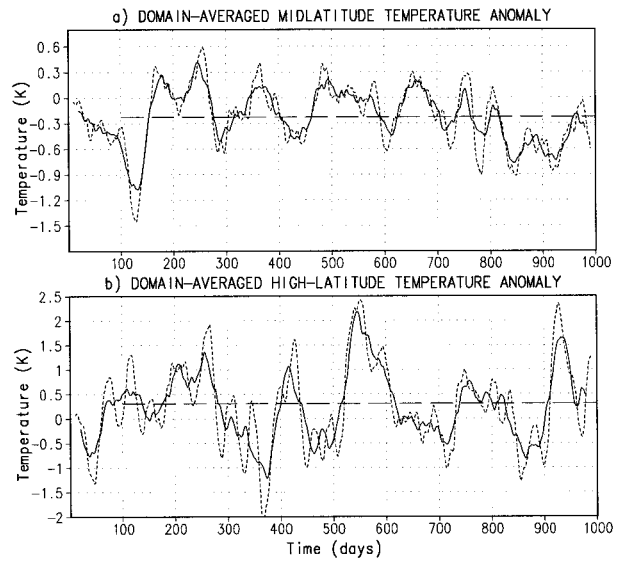


FIG. 8. Time series of domain-averaged temperature anomalies below 300 mb. (a) Midlatitude zonal-mean anomaly averaged from 40°N to 64°N. (b) High-latitude anomaly between 64° and 90°N. Data have been smoothed with 20-day (dashed) and 40-day (solid) moving averages. The time-mean values (long dashes) are for the last 900 days.

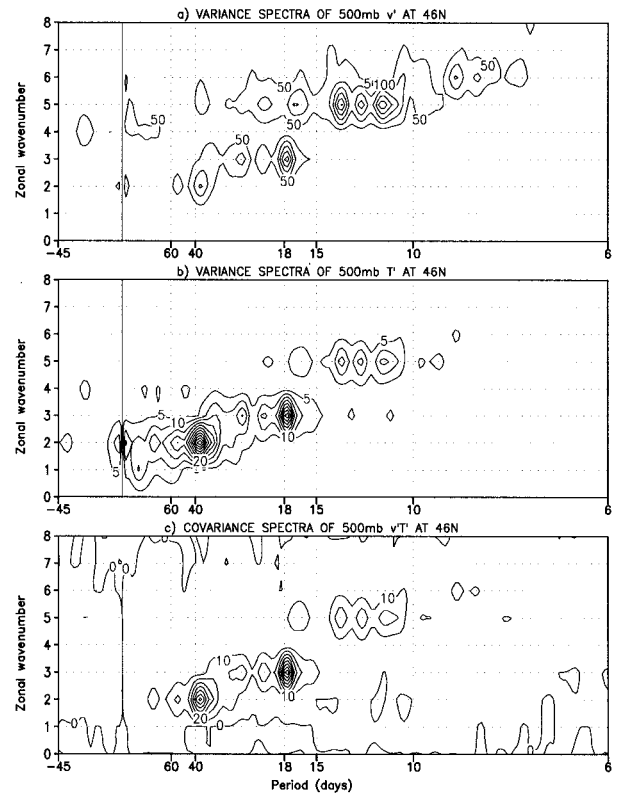


FIG. 9. Frequency and zonal-wave spectra of transient fluctuations at 500 mb and 46°N for case A: (a)  $v'^2$  with contour intervals of  $50 \text{ m}^2 \text{ s}^{-2} \text{ day}^{-1}$ , (b)  $T'^2$  with contour intervals of  $5 \text{ K}^2 \text{ day}^{-1}$ , and (c)  $v'T'$  with contour intervals of  $10 \text{ K m s}^{-1} \text{ day}^{-1}$ . The positive periods correspond to eastward propagating waves and negative values for westward propagation.

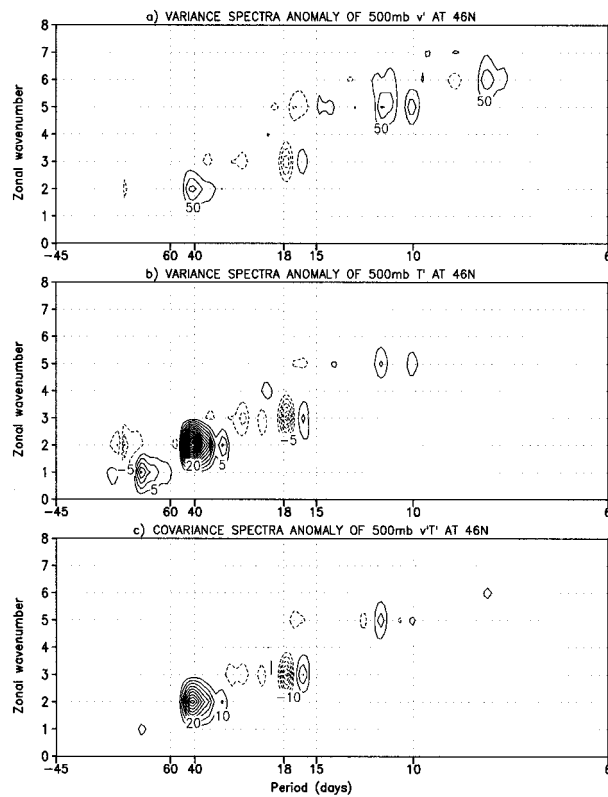


FIG. 10. Same as Fig. 9 except for anomalies (case B minus case A).

spectively. Despite the relatively long periods of 10–14 days, zonal wavenumber 5 essentially functions as a midlatitude “synoptic eddy” in this idealized model, as it is the fastest growing, baroclinically unstable wave that emerges from a randomly perturbed axisymmetric initial state. In the remaining work fluctuations with periods less than 15 days shall be referred to as synoptic eddies and those with longer periods as low-frequency waves. The spectra of  $T'$  and  $v'T'$  (Figs. 9b and 9c) show dominant peaks at low-frequency wavenumbers 2 and 3. Similar low-frequency waves also dominate the spectra of  $u'$  and  $u'v'$  in the upper troposphere near the subtropical jet (not shown).

Figure 10 shows that both synoptic-scale waves and low-frequency waves are enhanced with a stronger Hadley cell. The variance spectra of  $v'$  are enhanced at synoptic-scale wavenumber 5 with periods of 10–11 days, at wavenumber 6 with a period of 8 days, and at the low-frequency wavenumber 2 with a period of 40 days. By comparison, the enhanced power in  $T'$  and  $v'T'$  is concentrated at wavenumber 2 with a period of 40 days, where the power is more than doubled compared with case A. Although the dominance of wavenumber 2 in the spectral of  $T'$  partly reflects that the vertically integrated  $T'$  is related to  $v'$  divided by the zonal wavenumber, these results together with Fig. 8 suggest that the time-mean extratropical temperature

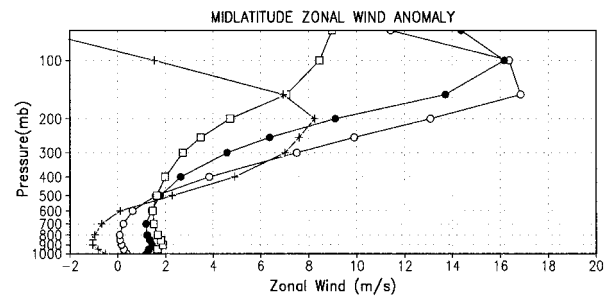


FIG. 11. Zonal wind anomalies (case B minus case A in  $\text{m s}^{-1}$ ) at 34°N (plus signs), 38°N (open circles), 42°N (solid circles), and 46°N (open squares).

anomalies involve an amplification of the low-frequency wavenumber 2. As noted earlier, low-frequency planetary waves can arise from baroclinic instability. An eastward propagating wave at zonal wavenumber 2 with a period of 40 days in the presence of westerlies would have a phase speed of less than  $10 \text{ m s}^{-1}$  and a steering level in the lower troposphere, characteristic of an unstable baroclinic wave.

To verify that wavenumber 2 is unstable in the presence of thermal damping and boundary-layer dissipation, we performed an analysis of the linear stability of the time-averaged zonal-mean state ( $u$ ,  $v$ ,  $T$ , and  $p_s$ ) including these damping terms. In order to obtain matrices that are computationally manageable, the resolution was reduced to 11 sigma levels and 44 latitudinal points. Of the 1496 eigenvectors for zonal wavenumber 2, 68 were found to be unstable with a maximum  $e$ -folding time of 5.97 days in case A, and 42 were unstable with a maximum  $e$ -folding time of 9.2 days in case B. These results, though not obtained at the full GCM resolution, serve to illustrate that zonal wavenumber 2 is unstable, with  $e$ -folding growth times comparable to those for wavenumber 5 (roughly 5.1 days in both cases). However, the closest match of the periods of these unstable modes to 40 days is 46 days, and there are significant structural changes between the eigenvectors in cases A and B. Moreover, the preferential amplification of wavenumbers 2 and 5 in case B cannot be predicted based on their growth rates. Even if these waves are baroclinically unstable, some type of selection or amplification mechanism would still be required. Given that nonlinear interaction is essential for flow equilibration, which entails structural modifications of these linear eigenmodes, it is not clear how the wavenumber 2 in the equilibrated climate is related to these unstable eigenmodes (DelSole and Hou 1998, manuscript submitted to *J. Atmos. Sci.*). The main point of this analysis is to verify that wavenumber 2 can spontaneously arise from internal dynamics.

### c. Dynamic adjustments outside the Tropics

The key supposition that a stronger Hadley cell can increase the baroclinicity outside the Tropics is con-

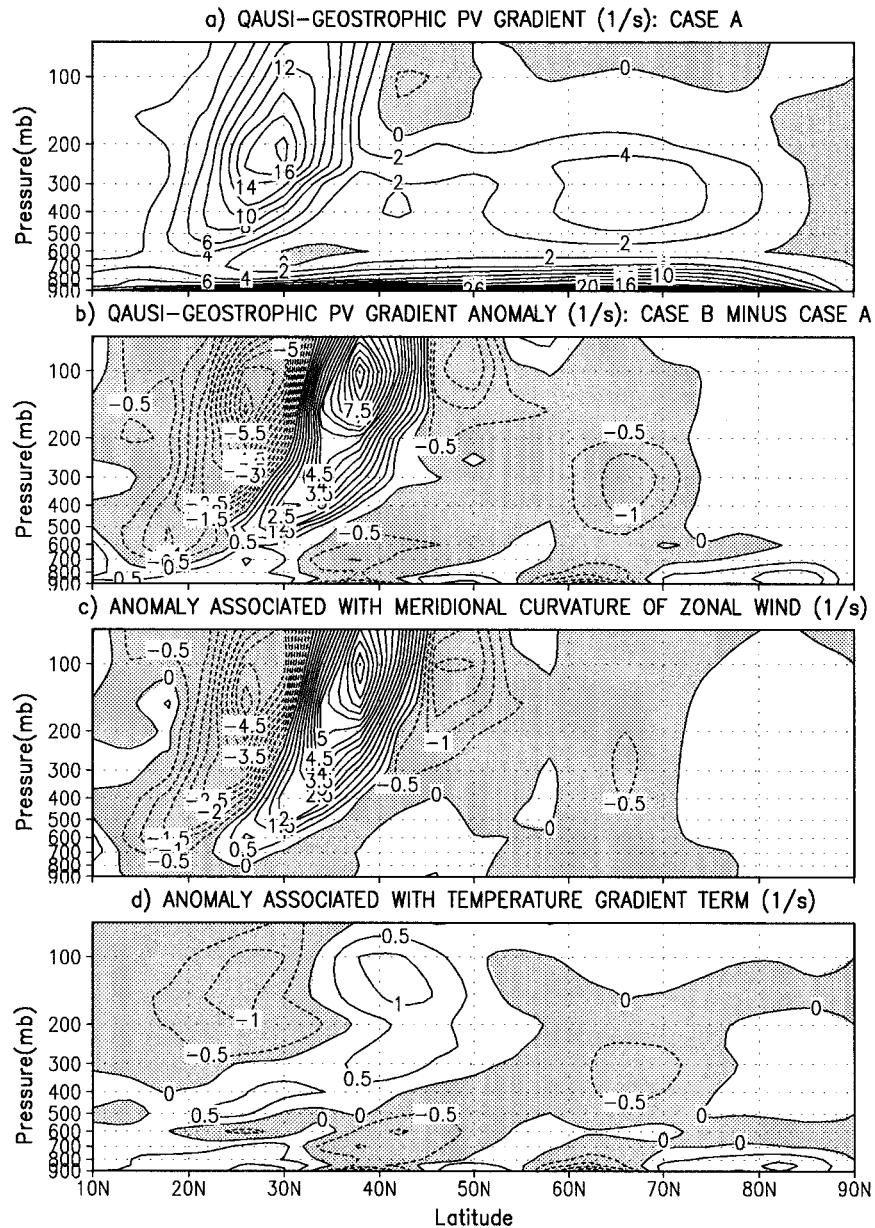


FIG. 12. (a) Zonally averaged quasigeostrophic PV gradient (in units of  $s^{-1}$ ) averaged over the last 900 days for case A. (b) PV gradient anomaly in units of  $s^{-1}$  (case B minus case A). (c) PV gradient anomaly associated with the meridional curvature of  $u$  [the second term in Eqn. (2)]. (d) PV gradient anomaly associated with the third term in Eq. (2).

firming in Fig. 11, which shows increased vertical shear of the zonal wind from the subtropics to nearly  $50^{\circ}N$  (also see Fig. 4). At  $38^{\circ}N$  the increased zonal wind shear between 150 mb and the surface is about  $17 \text{ m s}^{-1}$ , or 28% of the shear in case A. This increased midlatitude zonal wind shear is accompanied by enhanced variance of transient eddies shown in Fig. 10. A dynamical implication of the stronger zonal wind shear outside the Tropics is that it alters the meridional gradient of the quasigeostrophic potential vorticity, hence the quasigeostrophic index of refraction in upper troposphere

(Nigam and Lindzen 1989), which would imply modifications in the quasigeostrophic eddy structures and the resulting poleward heat transport. The zonally averaged quasigeostrophic PV gradient,  $[q_y]$ , in the pressure coordinate is (Edmon et al. 1980)

$$[q_{\phi}] = 2\Omega \cos\phi - [(a \cos\phi)^{-1}(u \cos\phi)_{\phi}]_{\phi} + f([\theta_{\phi}]/[\theta_p])_p, \tag{1}$$

where  $2\Omega \cos\phi$  is the planetary vorticity gradient,  $a$  is the earth's radius,  $f$  is the Coriolis parameter,  $\theta$  is po-

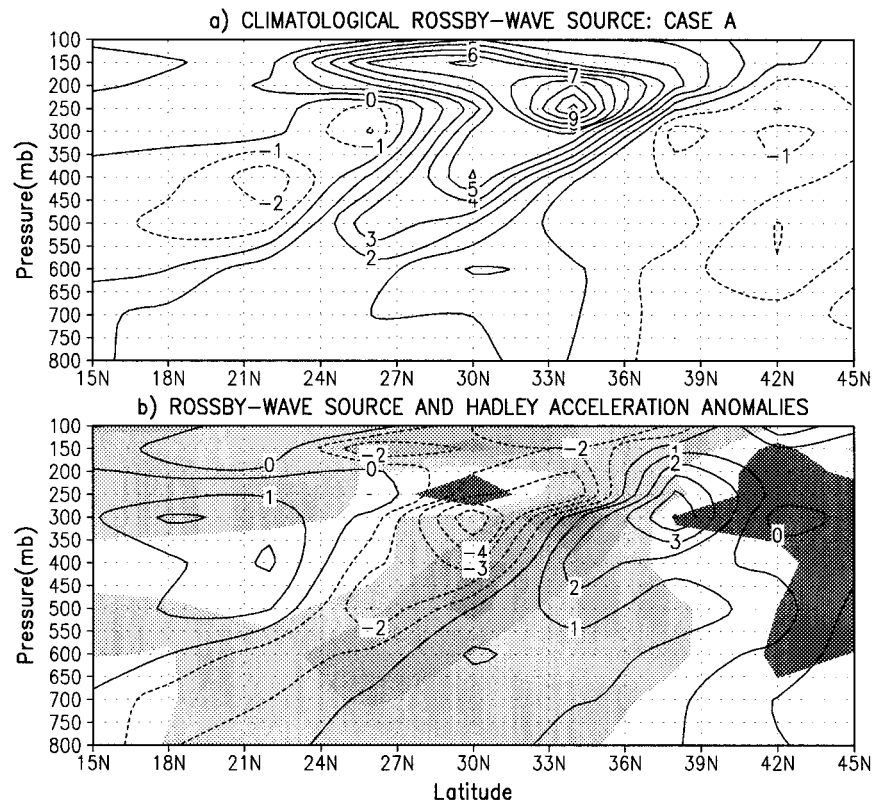


FIG. 13. (a) Zonally averaged "Rossby wave source" in units of  $10^{-11} \text{ s}^{-2}$  averaged over the last 900 days for case A. (b) Rossby wave source anomaly (contours) in  $10^{-11} \text{ s}^{-2}$  superimposed on averaged Hadley acceleration anomaly (shaded). Positive values of acceleration anomaly are shown in light shades in increments of  $0.5 \text{ m s}^{-1} \text{ day}^{-1}$ ; the dark shade corresponds to values less than  $-0.5 \text{ m s}^{-1} \text{ day}^{-1}$  (see Fig. 5 for details).

tential temperature, and  $p$  is pressure. Figure 12 shows that the upper-tropospheric PV gradient maximum associated with the subtropical jet is shifted poleward in case B, leading to enhanced midlatitude PV gradients between  $32^\circ$  and  $45^\circ\text{N}$ . This is due mainly to changes in the meridional curvature of  $u$  (Fig. 12c). The PV gradients in the middle and lower troposphere are reduced, due primarily to the third term in (1), which is consistent with enhanced PV mixing by baroclinic eddies (Held and Hoskins 1985). Also significant is that, in the high latitudes, there is a well-defined reduction in the midtropospheric PV gradient centered at  $65^\circ\text{N}$ , which coincides with the region of reduced meridional temperature gradient shown in Fig. 7. This high-latitude PV gradient reduction, which implies increased PV mixing by transient eddies, may be viewed as the dynamic adjustment associated with the midlatitude cooling and high-latitude warming anomalies.

The enhanced baroclinicity in the midlatitudes is the net result of a stronger poleward absolute vorticity flux by a stronger Hadley cell and deceleration by midlatitude eddies. In this region of increased zonal wind shear, balance between the mean-flow acceleration by the eddy-induced MMC and that by eddies also changes, as

can be seen in Fig. 5. For instance, at 200 mb, the level of maximum horizontal divergence in the upper troposphere, the steady-state zonal momentum equation is given approximately by  $[v][\zeta] \approx -[v'\zeta']$ , where  $\zeta$  is the absolute vorticity and the brackets denote a time-averaged zonal mean on isobaric surfaces. The midlatitude negative anomaly in  $[v][\zeta]$  at 200 mb in Fig. 5c implies an increase in the poleward flux of  $\zeta$  by transient eddies.

Since the circulation outside the Tropics is governed by vorticity dynamics, the time-mean changes must represent a steady-state adjustment of the vorticity field to a stronger Hadley cell. In a steady-state, the divergent circulation is related to the rotational flow via the vorticity equation:

$$\mathbf{V}\psi \cdot \nabla \zeta = -\nabla \cdot (\mathbf{V}_\chi \zeta) = -\mathbf{V}_\chi \cdot \nabla \zeta - \zeta \nabla \cdot \mathbf{V}_\chi \equiv S, \quad (2)$$

where  $\mathbf{V} = (u, v)$ ,  $\nabla$  is the horizontal gradient operator, the subscripts  $\psi$  and  $\chi$  denote the rotational and divergent components of the flow, respectively. The rhs of (2), that is, the ageostrophic advection of absolute vorticity and vorticity stretching due to horizontal divergence, has been referred to as the "Rossby wave source"  $S$  (Sardeshmukh and Hoskins 1988). Equation

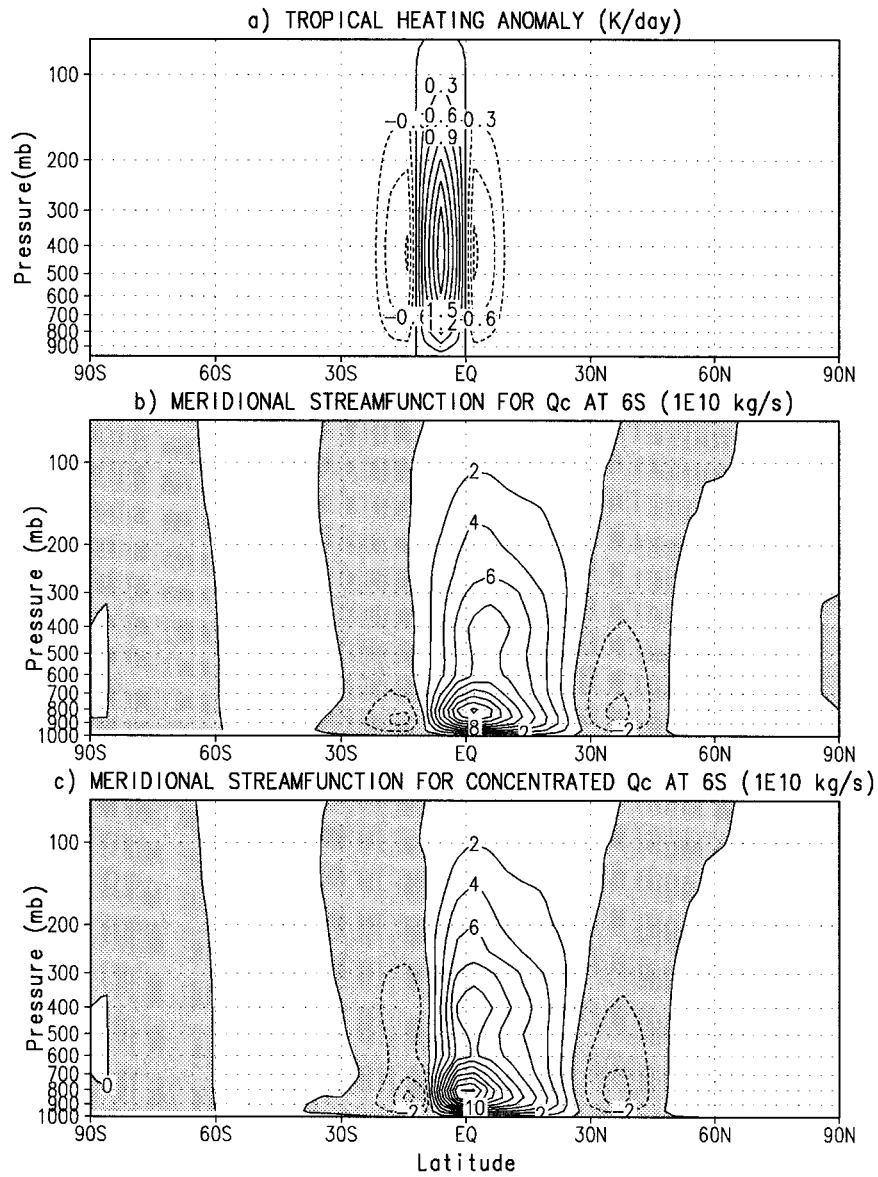


FIG. 14. (a). Anomaly in  $K\ day^{-1}$  due to concentration of the prescribed tropical heating at  $6^{\circ}S$  (case C minus case B). (b) The meridional streamfunction in units of  $10^{10}\ kg\ s^{-1}$  averaged over the last 900 days for case B. (c) Corresponding streamfunction for case C.

(2) provides a diagnostic relation between the advection of absolute vorticity by the rotational flow  $\mathbf{V}_{\psi}$  and the divergence of the absolute vorticity flux by  $\mathbf{V}_x$ . While within the Hadley cell domain  $\mathbf{V}_x$  is primarily thermally controlled (as demonstrated by the equal-area solution),  $\mathbf{V}_x$  at the poleward edge of the winter cell and beyond is influenced by midlatitude eddies. Figure 13 shows that the changes in the time-averaged  $[S]$  consist of a horizontal dipole anomaly, corresponding to a poleward shift of the subtropical maximum in the zonal-mean advection of vorticity by the rotational flow. This dipole anomaly in  $[S]$  coincides with the westerly acceleration

anomaly along the poleward edge of the Hadley cell due to a weakened deceleration of  $[u]$  by the eddy-induced MMC (see Fig. 5). Since  $[S]$  is the meridional gradient of the zonally averaged absolute vorticity flux by the divergent circulation, this suggests that  $[S]$  is dominated by the horizontal gradient of  $[v][\zeta]$ , which is consistent with this  $[S]$  dipole anomaly reflecting mainly the changes in the vorticity stretching term (not shown). According to (2), this subtropical dipole anomaly in  $[S]$  may also be interpreted as a steady-state adjustment in the advection of absolute vorticity by the rotational flow associated with an enhanced subtropical

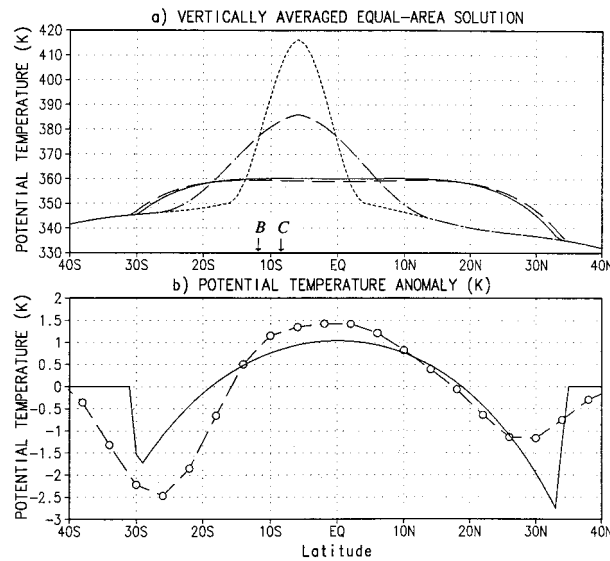


FIG. 15. (a) "Equal-area" solutions for the vertically averaged potential temperature (dashed for case B; solid for case C). Also shown are the prescribed thermal-equilibrium potential temperatures for cases B (dash-dots) and C (dots). The difference between the mean potential temperature its thermal equilibrium profile is a measure of the vertically averaged diabatic heating. The arrows labeled B and C mark the boundary between the winter and summer cells in cases B and C, respectively. (b) Comparison of the equal-area solution for the vertically averaged potential temperature anomaly (solid) with the 500-mb potential temperature anomaly from GCM simulations (dashed).

convergence due to a stronger Hadley cell, which is seen in Fig. 13b as a positive  $[S]$  anomaly between  $15^{\circ}$  and  $24^{\circ}$ N above 500 mb.

#### 4. Results for a narrowly concentrated tropical heating

Results in the previous section showed that a stronger Hadley circulation can lead to a reduction of extratropical temperature gradient rather than an equatorward shift of the global heating pattern, as found by Chang (1995) for a narrowly concentrated tropical heating. To reconcile our finding with Chang's experiment, we performed a 1000-day simulation for a tropical heating concentrated at  $6^{\circ}$ S while preserving the total heat input (case C in section 2), similar to the heating perturbation used in Chang. The tropical heating anomaly (case C minus case B) and the meridional streamfunctions are shown in Fig. 14. For a narrow heating, the winter Hadley cell is more intense, consistent with the equal-area Hadley cell solution of Hou and Lindzen (1992) and the GCM simulation of Chang. But the intensification of the winter cell through heating concentration is less than that in case B and confined mainly to the region of the narrow heating. In Fig. 15a the equal-area solution for case C shows an enhanced diabatic heating in the Tropics, accompanied by a slight contraction of the winter

Hadley cell (relative to case B), with the Hadley cell boundaries given by

$$\phi_0 = 8.74^{\circ}\text{S}, \quad \phi_s = 29.79^{\circ}\text{S}, \quad \text{and}$$

$$\phi_w = 33.41^{\circ}\text{N}. \quad (\text{case C})$$

Since the averaged vertical velocity is proportional to the averaged diabatic heating in the region of ascending motion, the intensification and contraction of the rising branch of the winter cell are evident. In the winter hemisphere, this contraction is seen as an equatorward shift of the area of the rising motion. Figure 15b shows that the 500-mb temperature anomalies in the Tropics and subtropics are predicted by the equal-area solution.

The time-averaged zonal-mean temperature anomaly is shown in Figs. 16a and 16b. In the winter extratropics the warming between  $40^{\circ}$ N and  $60^{\circ}$ N is statistically significant but not the cooling over the winter pole. This agrees with Chang's southern-winter result and can be compared with his Fig. 4b. The main difference is that the extratropical warming in Chang's case is farther poleward at  $60^{\circ}$ S, which may be related to the fact that his winter jet is also farther poleward, at  $45^{\circ}$  instead of  $30^{\circ}$ .

Since the temperature anomaly in Fig. 16 is opposite in sign to that shown in Fig. 3, a deceleration of the winter subtropical jet is expected according to the analysis of section 3. This is confirmed in Fig. 16c, which shows a region of weak deceleration by the MMC in the upper troposphere from  $10^{\circ}$  to about  $30^{\circ}$ N. The relationship between the subtropical acceleration and the extratropical temperature anomaly is therefore consistent with the results of section 3, except that here the reduced poleward heat transport between the mid and high latitudes is not statistically significant due to the weak subtropical deceleration anomaly (above 200 mb and equatorward of  $30^{\circ}$ N), whose magnitude is less than one-fifth of its counterpart in case B. The statistically robust warming immediately poleward of the jet in Fig. 16 reflects an adjustment in the temperature field in balance with changes in the zonal wind, as discussed in Chang. The absence of a significant high-latitude response also supports the interpretation that dynamic transport between mid- and high latitudes cannot account for all of the midlatitude cooling anomaly in case B.

Figure 17a shows that the zonal wind shear is slightly reduced in the midlatitudes but increased between  $10^{\circ}$  and  $30^{\circ}$ N, consistent with an equatorward shift of the jet. But given the small magnitudes of these changes, the actual shift is imperceptible. Figure 17b shows that the upper-tropospheric PV gradient anomalies are opposite to those in case B. Also, there is no meaningful midtropospheric PV gradient anomaly in the high latitudes, unlike the situation in case B. The absence of this high-latitude PV gradient anomaly together with the lack of a robust high-latitude temperature anomaly support the interpretation that a change in the poleward

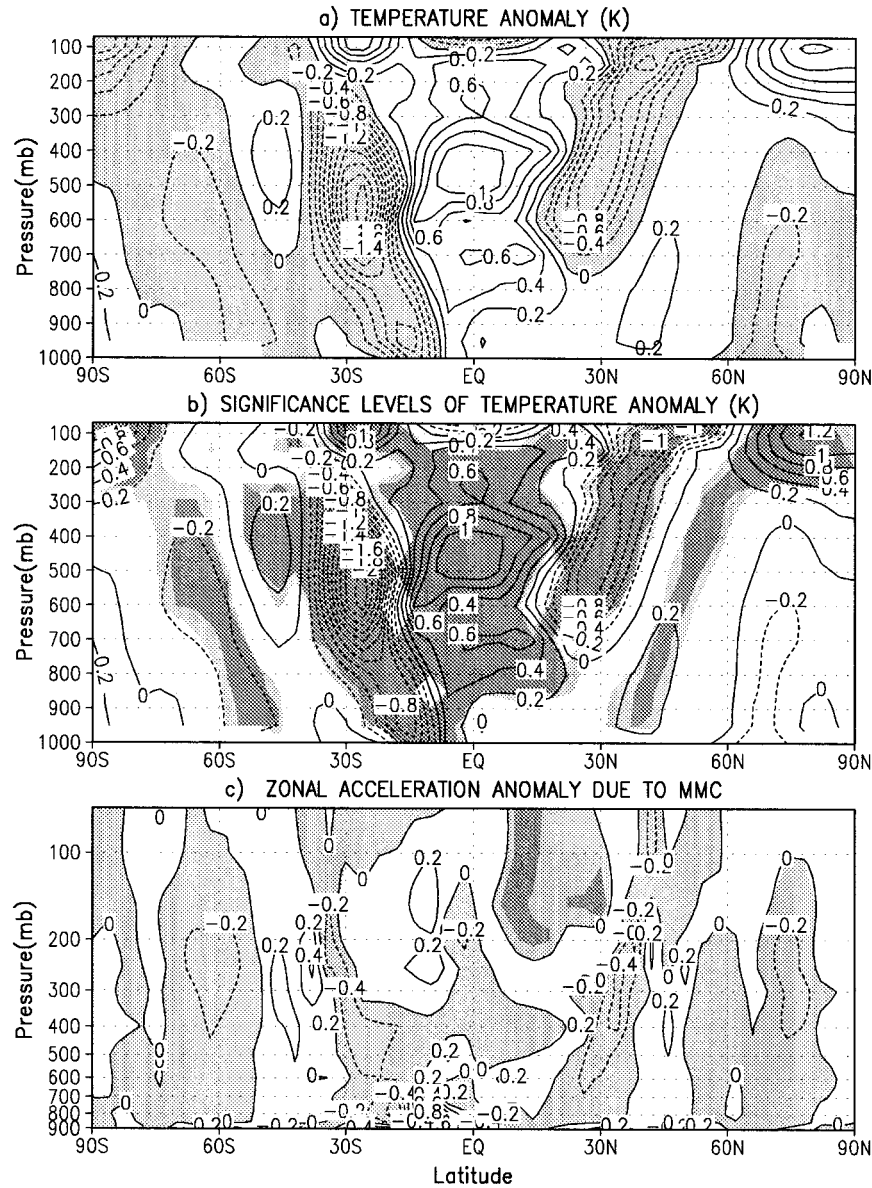


FIG. 16. (a) Time-averaged zonal-mean temperature anomaly in kelvins per day (case C minus case B) for the last 900 days. (b) Significance levels of the anomaly based on Student's *t* test. The light-shade regions exceed 95% and the dark-shade regions exceed 99%. (c) Time-averaged zonal acceleration anomaly due to the mean-meridional circulation for the last 900 days. (The units are  $\text{m s}^{-1} \text{ day}^{-1}$ .) The dark shade in the northern subtropics indicates values between  $-0.05$  and  $-0.1 \text{ m s}^{-1} \text{ day}^{-1}$ .

heat transport between the middle and high latitudes is associated with a change in the quasigeostrophic PV gradient. Figure 17c shows that the subtropical deceleration by the MMC is associated with a dipole anomaly in  $[S]$  opposite in sign to that in case B (Fig. 13), corresponding to an equatorward shift of the subtropical maximum in  $[S]$ .

Chang linked the equatorward shift of the winter jet with an enhanced acceleration by the MMC in the Tropics (between  $10^{\circ}\text{S}$  and  $20^{\circ}\text{S}$  in his Fig. 12a) and

was able to reproduce the extratropical anomaly by applying an artificial westerly acceleration in this region. However, in this study the positive acceleration anomaly induced by the MMC is negligible and confined close to the equator (Fig. 16c), suggesting that the equatorward shift of the subtropical jet should be associated with the deceleration in the *subtropics*. This "subtropical" deceleration is also evident in Chang's Fig. 12a, except that it occurs farther poleward between  $30^{\circ}\text{S}$  and  $50^{\circ}\text{S}$  since his winter jet is

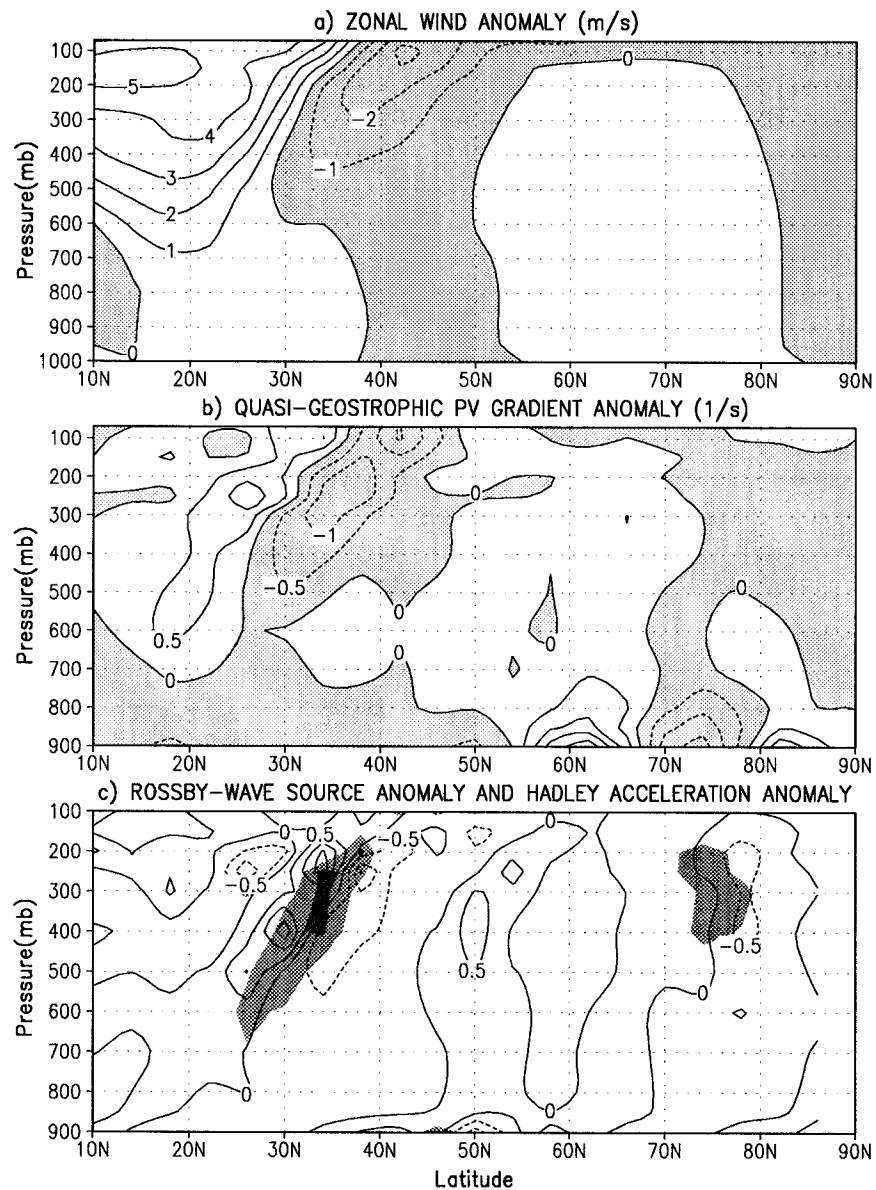


FIG. 17. (a) Zonally averaged zonal wind anomaly in meters per second (case C minus case B) averaged over the last 900 days. (b) Zonally averaged quasigeostrophic PV gradient anomaly (in units of  $\text{s}^{-1}$ ) for the same period. (c) Time-averaged zonal-mean Rossby wave source anomaly in contour intervals of  $0.5 \times 10^{-11} \text{ s}^{-2}$  superimposed on Hadley acceleration anomaly for the last 900 days. Negative values of acceleration anomaly are shaded in increments of  $0.2 \text{ m s}^{-1} \text{ day}^{-1}$ .

at  $45^{\circ}\text{S}$ . This interpretation is consistent with the results in section 3, which showed no evidence of tropical deceleration associated with a poleward displacement of the jet, while the subtropical acceleration is quite prominent in Fig. 5. This suggests that in Chang's prescribed "tropical westerly acceleration" experiment, the winter Hadley cell must respond by advecting less angular momentum poleward in order to satisfy thermodynamic constraints, resulting in a net deceleration poleward of  $30^{\circ}$  in the winter subtropics.

### 5. Application to assimilated atmospheric data

The results of the previous sections were based on perpetual-winter simulations of an idealized GCM with a zonally symmetric forcing and no orography. The extent to which they may be applicable to the observed atmosphere is tested by examining the NASA GEOS-1 assimilated global dataset, which has a horizontal resolution of  $2^{\circ}$  lat  $2.5^{\circ}$  long, with 14 upper-air pressure levels plus the sea level (see Schubert et al. 1995). This reanalysis was produced initially for 1985–89 but has

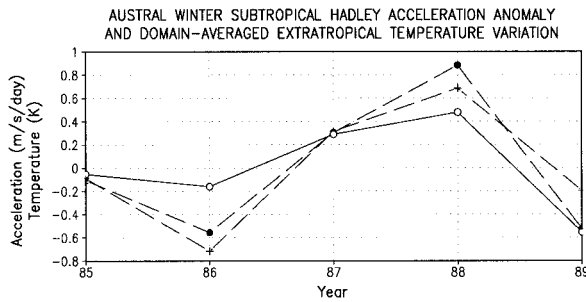


FIG. 18. Domain-averaged subtropical Hadley acceleration anomaly and extratropical temperature anomalies for the 1985–89 austral winters. Anomalies are departures from the 5-yr mean. The Hadley acceleration anomaly averaged from 150 to 200 mb and 20° to 28°S is labeled with open circles. The high-latitude temperature anomaly below 400 mb averaged from 60° to 90°S is the dashed line labeled with plus signs. The proxy for the extratropical temperature gradient anomaly below 400 mb given in terms of the domain-averaged high-latitude temperature anomaly minus the midlatitude anomaly averaged from 40° to 60°S is given by dashes labeled with solid circles.

since been extended to 1979–93. Although the assimilation system remained fixed throughout this period, data selection and quality control have introduced variability and inhomogeneity in the observations ingested by the system (Park et al. 1996). To minimize the impact of data inhomogeneity, we used the initial 1985–89 period in this study. Moreover, since stationary waves are weak in the southern extratropics, we will apply the transient-eddy diagnostics developed in section 3 only to austral winters.

The GEOS-1 reanalysis shows significant variations in the intensity of the austral winter (i.e., June, July, and August) Hadley cell. From 1985 to 1989, the yearly values of the maximum streamfunction are  $-20$ ,  $-19$ ,  $-23$ ,  $-22$ ,  $-20$  in units of  $10^{10} \text{ kg s}^{-1}$ , respectively. These are in good agreement with those derived from the upper-air wind observations (Oort and Yienger 1996, their Fig. 5). In particular, the strength of the austral winter Hadley cell peaks in 1987 in both analyses. In the GEOS-1 reanalysis, the comparatively strong austral winter Hadley circulations in 1987 and 1988 are associated with a higher than normal zonal-mean surface temperature maximum to the north of the equator during these El Niño and La Niña years.

Over this 5-yr period, the subtropical Hadley acceleration averaged from 150 to 200 mb and 20° to 28°S is the strongest in 1988 (despite the streamfunction maximum being stronger in 1987). This area-averaged subtropical Hadley acceleration, in units of  $\text{m s}^{-1} \text{ day}^{-1}$ , is 2.21 for 1988, 2.02 for 1987, 1.68 for 1985, 1.57 for 1986, and 1.17 for 1989. These values vary by a factor of 2 over this five-year period. The analysis of section 3 suggests that a stronger than normal subtropical Hadley acceleration should be accompanied by a smaller extratropical temperature gradient and a warm temperature anomaly in the high latitudes. This is confirmed in Fig. 18, which shows interannual variations of the

averaged subtropical Hadley acceleration anomaly and polar temperature anomaly for the five austral winters from the GEOS-1 reanalysis. The anomaly correlation between the subtropical Hadley acceleration and the winter high-latitude temperature (averaged from 400 to 950 mb and 60° to 90°S) is 0.76 according to Pearson's  $r$  or 0.80 by the more stringent, nonparametric Kendall's  $\tau$  analysis (with a probability of zero correlation of 0.05). Similarly, when the subtropical acceleration is correlated with a proxy for the extratropical temperature gradient given in terms of the difference between the domain-averaged high-latitude temperature and the midlatitude temperature (averaged from 400 to 950 mb and 34° to 60°S), the correlation is 0.92 according to Pearson's  $r$  (with a probability of 0.03), or 0.80 according to Kendall's  $\tau$  (with a probability of 0.05).

The zonally averaged cross sections of subtropical Hadley acceleration and austral winter temperature anomalies are shown in Fig. 19 for two extreme cases: 1988 for a strong positive subtropical Hadley acceleration anomaly and 1989 for a negative acceleration anomaly. In Figs. 19a and 19c the Hadley acceleration anomalies are shown for the subtropical region surrounding the averaging area used for Fig. 18. Also shown in these figures are the zonal wind anomalies. In 1988, the increased vertical shear between 30° and 45°N clearly reflects a poleward shift of the subtropical jet, similar to that in case B of the idealized GCM experiment. In 1989 the subtropical zonal wind shear is reduced, which is consistent with the cold polar temperature, but there is no apparent shift associated with this reduction. Figure 20 shows that during the 1988 winter with the strong Hadley cell, the variance spectra of the midlatitude 500-mb geopotential height show an enhanced low-frequency response at wavenumbers 2–3 that peaks between 40 and 60 days, similar to the idealized GCM result. There is, however, no evidence of enhanced synoptic-scale activity, suggesting that only low-frequency transients are responsible for the extratropical temperature anomalies.

The idealized GCM results also showed that the temperature anomalies in the middle and high latitudes are associated with a change in the tropospheric meridional PV gradient across the boundary of the cooling and warming anomalies. This is evident in Fig. 21, despite the noisy results near the winter pole and close to the surface. During the 1988 austral winter, the PV gradients are reduced between 40° and 70°S, with a maximum reduction near 400 mb, where the climatological PV gradient is the strongest. In the subtropics, the anomaly is consistent with a poleward shift of the subtropical PV gradient maximum, similar to that described in case B. In contrast to this, the PV gradients are sharpened between 50° and 75°S in 1989. These regions of PV gradient adjustments also appear to follow the boundaries of the temperature anomalies shown in Figs. 19b and 19d.

These results show that the connection between the

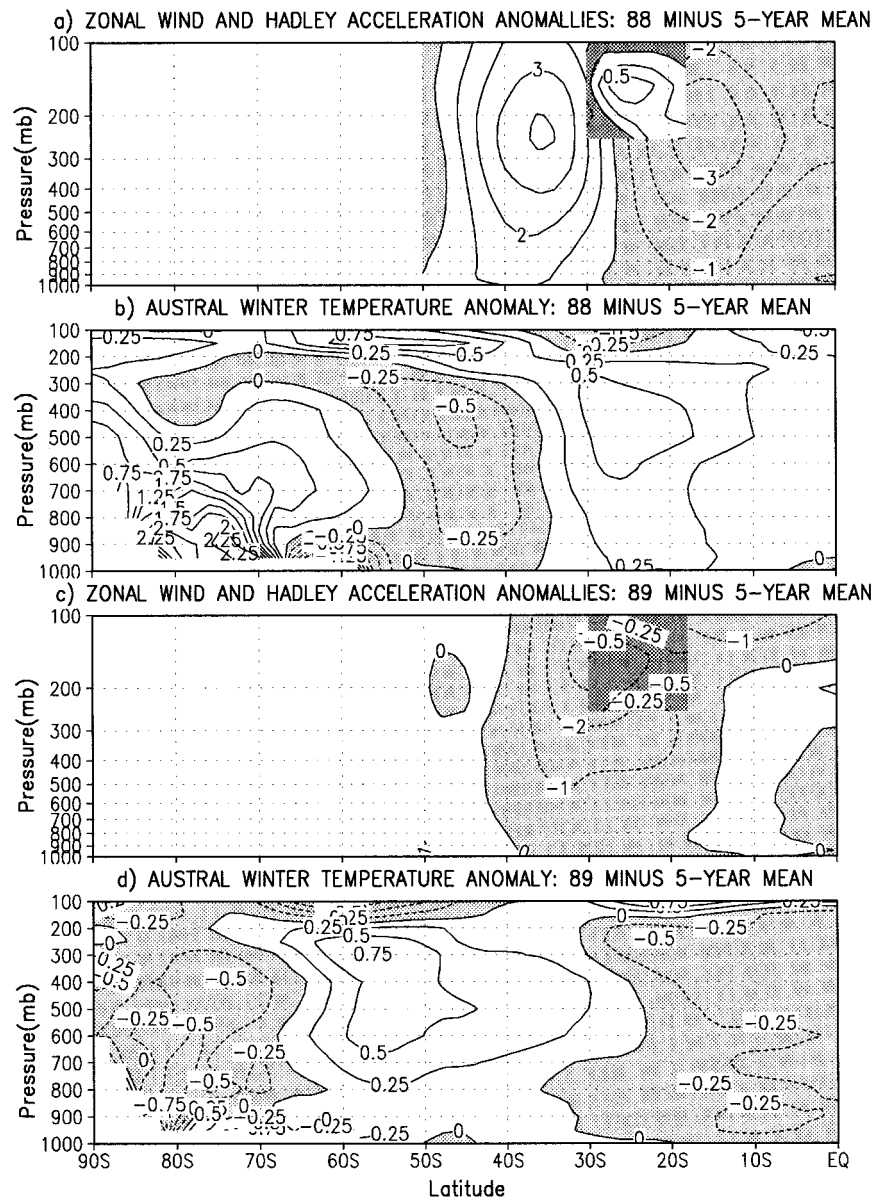


FIG. 19. (a) Austral winter zonal wind and subtropical Hadley acceleration anomalies showing the difference between 1988 and the 5-yr mean in the GEOS-1 reanalysis. The acceleration anomaly is shown for the region between  $18^{\circ}$  and  $30^{\circ}\text{N}$  and from 100 mb to 250 mb, in contours of  $0.25 \text{ m s}^{-1} \text{ day}^{-1}$ , with negative values indicated in dark shade. The zonal wind is shown in contours of  $1 \text{ m s}^{-1}$ , with negative values in light shade. (b) Corresponding austral winter temperature anomaly (in K) for 1988. (c) Same as (a) except for 1989. (d) Same as (b) except for 1989.

subtropical Hadley acceleration, zonal wind shear, and the extratropical temperature and PV gradients found in the idealized GCM experiments are also in the GEOS-1 reanalysis for the five austral winters from 1985 to 1989. Compared with the GCM results, although the changes in the PV gradient and zonal wind shear in the subtropics are smaller in the GEOS-1 reanalysis, the temperature and PV gradient anomalies in the high latitudes are comparable. The implication is that the mid- and high-latitude PV mixing by eddies

in the atmosphere may be more sensitive to changes in the subtropical jet. That diagnostics derived from idealized GCM experiments are useful for analyzing the assimilated atmospheric data suggests that the idealized GCM, despite its simplifications, still captures the essential physics. Considering that significant differences exist between the simple model and the real atmosphere (e.g., the tropical heating is not zonally symmetric), the similarities between the reanalysis and GCM results suggest that the hypothesized connection

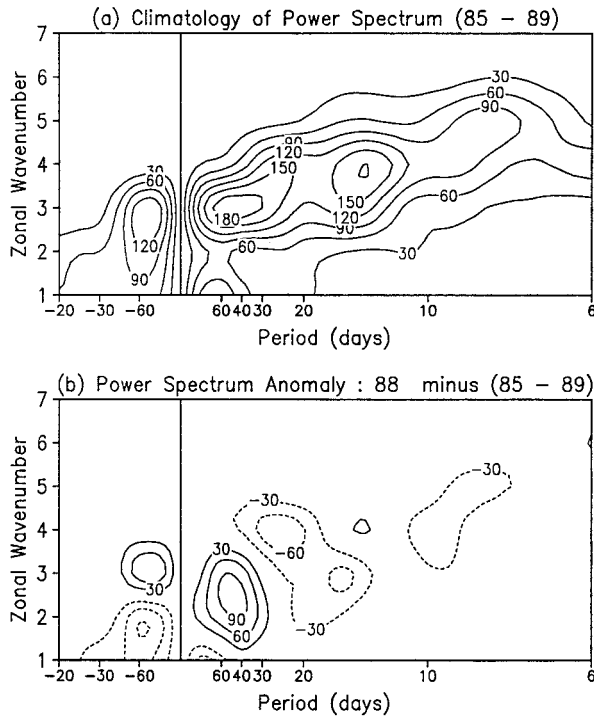


FIG. 20. Power spectrum of the 500-mb geopotential height averaged from  $40^{\circ}$  to  $60^{\circ}$ S from the GEOS-1 DAS reanalysis. (a) Climatology for austral winters from 1985 to 1989. The analysis is based on 120-day time series beginning on 16 May. (The units are in  $m^2$ .) (b) Corresponding anomaly showing the difference between 1988 and the 5-yr mean.

between the tropical circulation and the extratropical climate is fairly robust.

## 6. Summary and conclusions

We have examined the hypothesis that the strength of the Hadley circulation can affect the baroclinicity in the subtropics and modulate the temperature gradient between the middle and high latitudes. We have tested this in a series of idealized GCM experiments and by examining the GEOS-1 reanalysis from 1985 to 1989. The GCM results show that, if the changes in the Hadley cell are such that the mean meridional circulation produces a westerly acceleration in the winter subtropics, the time-averaged zonal wind would have stronger vertical shears between the subtropics and the midlatitudes and the temperature gradient between the mid- and high latitudes would decrease in the winter extratropics—as in the example of a Hadley cell intensified through a tropical heating shift toward the summer pole. But, if the Hadley circulation is intensified through a latitudinal concentration of heating in the summer Tropics, the changes can lead to a deceleration of the subtropical jet and a stronger temperature gradient in the winter extratropics.

The midlatitude temperature response to a subtropical

Hadley acceleration anomaly is dominated by enhanced power in low-frequency planetary-scale waves that peaks at zonal wavenumber 2 with a period of 40 days. The modulation of the winter extratropical temperature gradient thus involves a change in the net heat transport by the low-frequency planetary-scale transients and the wave-induced mean meridional circulation. That the reduction in the extratropical temperature gradient is established over timescales much longer than the initial adjustment by the synoptic-scale eddies also argues against the latter being the primary vehicle for the extratropical response—unless it can be shown that synoptic eddies are responsible for the enhanced low-frequency response. However, linear stability analysis of the equilibrated zonal mean state shows that low-frequency planetary waves are baroclinically unstable, with growth rates comparable to those of synoptic-scale waves. The GCM results also show that the increased poleward heat transport implicit in the midlatitude cooling and high-latitude warming anomalies is associated with a reduced quasigeostrophic PV gradient, consistent with enhanced PV mixing by baroclinic eddies.

Application of the GCM-derived diagnostics to the GEOS-1 reanalysis from 1985 to 1989 reveals similar relations between interannual variations in the Tropics and changes in the extratropical climate. In particular, the year-to-year variation in the austral winter extratropical temperature gradient is correlated with the variation in the subtropical acceleration by the winter Hadley cell, with anomaly correlation coefficients ranging from 0.80 to 0.92, depending on the statistical test. The positive subtropical Hadley acceleration anomaly during the 1988 austral winter is accompanied by stronger zonal wind shears in the subtropics and midlatitudes, a colder than normal troposphere in the midlatitudes, and a warmer polar region. These extratropical temperature anomalies are associated with reduced PV gradients, and the midlatitude geopotential height anomaly at 500 mb shows a spectral peak at wavenumbers 2–3 with periods between 40 and 60 days, similar to the GCM results. The idealized GCM thus appears to contain the essential physics linking the tropical circulation to the extratropical temperature gradient.

The basic connections between the Hadley circulation and the zonally averaged climate in the winter extratropics are illustrated in Fig. 22. It shows that, as a stronger Hadley cell transports more absolute angular momentum into the subtropics, the equilibrated zonal wind has stronger vertical shears between the subtropics and the midlatitudes, which is accompanied by an increased poleward heat transport by transient eddies and the eddy-induced mean circulation, leading to a smaller temperature difference and reduced PV gradients between the middle and high latitudes.

Lastly, we note that the tropical–extratropical connection described in this work may be in some way related to global teleconnections in the presence of orography. The characteristic zonally averaged midlatitude

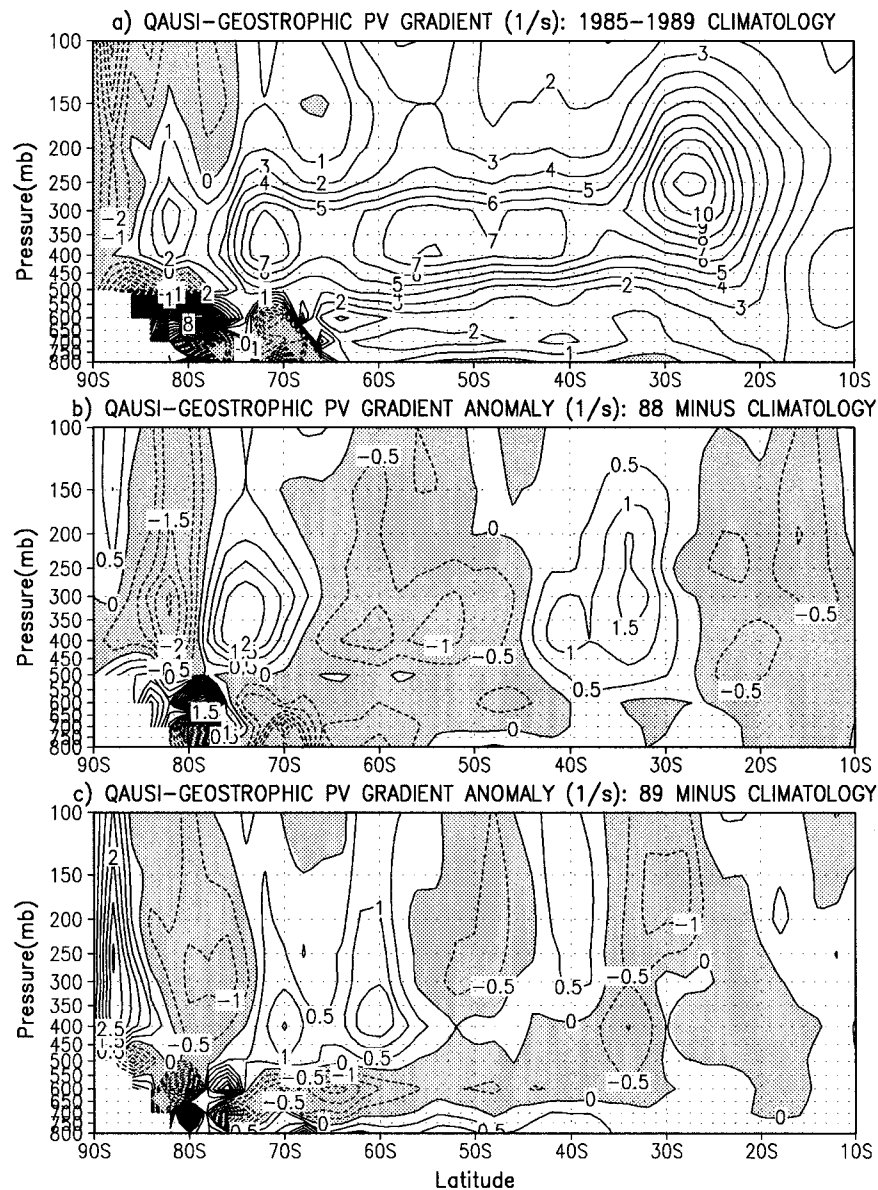


FIG. 21. (a) Zonally averaged quasigeostrophic PV gradient in units of  $s^{-1}$  averaged over five Austral winters (1985-89). (b) PV gradient anomaly (in units of  $s^{-1}$ ) for 1988 minus the 5-yr mean. (c) Same as (b) except for 1989.

cooling and high-latitude warming anomalies correspond to reduced surface pressure in the midlatitudes and increased surface pressure in the high latitudes. The study by Hou and Molod (1995) using the full GEOS GCM showed that when the intensification of the boreal winter Hadley circulation is dominated by heating anomalies in the western and central Pacific, the zonally averaged extratropical signal consists of a deepened surface low in the Gulf of Alaska and a weakened Icelandic low, similar to the teleconnection pattern described by Bjerknes (1966, 1969). Teleconnections associated with tropical heating anomalies and their propagation have been interpreted as barotropic wave trains (Wallace and

Gutzler 1981; Hoskins and Karoly 1981; Simmons et al. 1983; Hoskins and Jin 1991). But in this idealized GCM experiment with zonally symmetric forcing, it remains to be shown that such barotropic waves can carry much heat poleward. Alternatively, the extratropical temperature anomalies may result from the action of baroclinic waves in the presence of stronger subtropical zonal wind shears set up by a stronger Hadley cell. It has been proposed that teleconnections may be a response to changes in the sea surface temperature or regional land surface processes in the Tropics (Bjerknes 1969; Rowntree 1976), or associated with internal variability on intraseasonal or longer timescales (e.g., Lau

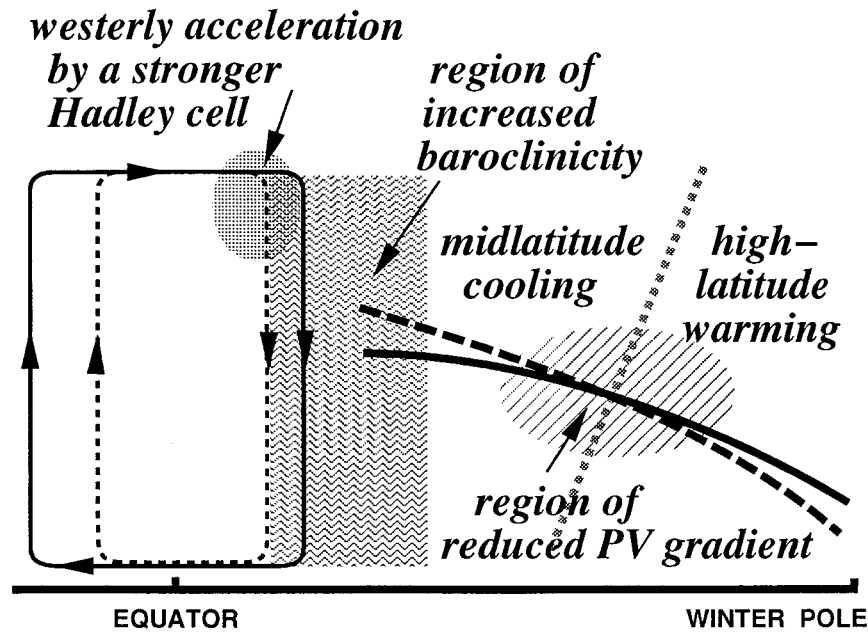


FIG. 22. A schematic showing that the intensification and poleward expansion of the cross-equatorial Hadley cell (solid with arrows) can lead to westerly acceleration in the subtropics and a region of enhanced vertical zonal wind shear extending from the subtropics into the midlatitudes. These anomalies are accompanied by a reduced meridional temperature gradient and a weaker potential vorticity gradient in the winter extratropics, which are consistent with enhanced PV mixing and increased poleward heat transport by baroclinic eddies.

1981). The present work raises the possibility that these ideas may be reconciled in terms of acceleration of the subtropical jet.

The results of this study suggest that tropical processes may play an active role in modulating the atmospheric heat transport from the subtropics to the high latitudes, which could have important implications for understanding climate variations ranging from intraseasonal variability to ice ages (Lindzen and Pan 1994). This work points to a subtle but potentially important aspect of climate sensitivity; namely, the extratropical temperature gradient may depend, in part, on the modulation of low-frequency planetary-scale transients by the divergent circulation in the Tropics, whose intensity and structure are sensitive to a small displacement of convective heating from the equator.

*Acknowledgments.* I would like to thank Prof. Richard Lindzen for encouragement and insightful discussions throughout this work, Drs. Isaac Held and Ka-Kit Tung for helpful comments, Dr. Timothy DelSole for the eigenanalysis code, and Dr. Wei Min for producing Fig. 20. This research was supported by the EOS Interdisciplinary Science Program, the NASA Research and Applications Program, and the Tropical Rainfall Measuring Mission Office through Grants 578-41-60-20 and 461-57-37-20.

APPENDIX

Reference Seasonal Climatology

The reference temperature,  $T_0(\phi, z)$ , comprises three terms, the first for simulating the effect of north-south differential heating, the second for controlling the mean vertical profile, and the third for representing diabatic heating effects in the midlatitudes; namely,

$$T_0(\eta, z) = \frac{\Delta(z)}{3}[1 - 3(\eta - \eta_0)^2] + T_r(z) + T_m(\eta, z), \tag{A1}$$

where  $\eta$  is the sign of latitude,  $z$  is the log-pressure height,  $z = H \ln(p_s/p)$ ,  $H$  is a scale height taken to be 8 km,  $p_s$  is a reference pressure of 1000 mb,  $\eta_0$  is the latitude at which  $T_0$  has a maximum, and  $\Delta(z)$ , which defines the equator-to-pole temperature for  $\eta_0 = 0$ , is given by  $\Delta_* \exp(-1.7z/z_T)$  for  $z < z_T$ , where  $\Delta_* = 40$  K and  $z_T$  is the height of convective heating at 100 mb.

The mean static stability is adjusted through  $T_r(z)$ , which has the form:

$$T_r(z) = T_r(0) + \left[ A - \frac{g}{C_p} \right] z + B \ln \left( \frac{\cosh\left(\frac{z - z_T}{h}\right)}{\cosh\left(\frac{z_T}{h}\right)} \right), \tag{A2}$$

where  $T_p(0) = 280$  K, and  $g/C_p$  is the dry adiabatic lapse rate. The parameters  $A$ ,  $B$ , and  $h$  are chosen to give zonal-mean values of  $N^2$  (the square of Brunt-Väisälä frequency) ranging from 1.4 to  $2 (\times 10^{-4} \text{ s}^{-2})$  below 300 mb everywhere outside the Tropics [which are somewhat larger than the observed values given by Lee and Mak (1994)]; namely,  $A = A_* \{1.13 + 0.3A_z(\eta - \eta_0)^2\}$ ,  $B = B_* h \{1 + 1.75B_z|\eta - \eta_0|\}$ , where  $A_* = 8 \times 10^{-3} \text{ K km}^{-1}$ ,  $A_z = \exp\{-[(z - z_s)/H]^4\}$ ,  $z_s = 22$  km,  $B_* = 4 \text{ K km}^{-1}$ ,  $B_z = \exp[-(z/(1.5z_T))^8]$ , and  $h = z_T$ . Above 300 mb,  $N^2$  rapidly increases to a maximum at 150 mb that varies from 5 to  $8.4 (\times 10^{-4} \text{ s}^{-2})$  between the subtropics and the poles.

The effects of diabatic heating in the midlatitudes are modeled by

$$T_m(\eta, z) = J \sum_{i=1,2} \cos^2\left(\frac{\pi(\eta - \eta_i)}{2\delta}\right) \times \sin\left(\pi\left(0.2 + 0.8\frac{z}{d}\right)\right) e^{z/H - 4z/z_T},$$

$$z < d, \quad \eta - \delta < \eta_i < \eta + \delta, \quad (\text{A3})$$

where  $J = 0.62 \times 10^{-5} \text{ K s}^{-1}$ ,  $\eta_1 = \sin(40^\circ)$ ,  $\eta_2 = \sin(-40^\circ)$ ,  $\delta = 0.34$  ( $20^\circ$  latitude) for  $\text{abs}(\eta) < \text{abs}(\eta_i)$ , otherwise  $\delta = 2(1 - \eta_i) \text{sgn}(\eta_i)$ ; and  $d = H[2.3 - 0.0145 \text{ abs}(\text{latitude in degrees})]$ .

#### REFERENCES

- Bjerknes, J., 1966: A possible response of the atmospheric Hadley circulation to equatorial anomalies of ocean temperature. *Tellus*, **18**, 820–829.
- , 1969: Atmospheric teleconnections from the equatorial Pacific. *Mon. Wea. Rev.*, **97**, 163–172.
- Blackmon, M. L., J. M. Wallace, N.-C. Lau, and S. L. Mullen, 1977: An observational study of the Northern Hemisphere wintertime circulation. *J. Atmos. Sci.*, **34**, 1040–1053.
- Chang, E. K. M., 1995: The influence of Hadley circulation intensity changes on extratropical climate in an idealized model. *J. Atmos. Sci.*, **52**, 2006–2024.
- Edmon, H. J., B. J. Hoskins, and M. E. McIntyre, 1980: Eliassen–Palm cross sections for the troposphere. *J. Atmos. Sci.*, **37**, 2600–2616.
- Held, I. H., and A. Y. Hou, 1980: Nonlinear axially symmetric circulations in a nearly inviscid atmosphere. *J. Atmos. Sci.*, **37**, 515–533.
- , and B. J. Hoskins, 1985: Large-scale eddies and the general circulation of the troposphere. *Advances in Geophysics*, Vol. 28A, Academic Press, 3–31.
- Holopainen, E. O., L. Rontu, and N.-C. Lau, 1982: The effect of large-scale transient eddies on the time-mean flow in the atmosphere. *J. Atmos. Sci.*, **39**, 1972–1984.
- Hoskins, B. J., and D. J. Karoly, 1981: The steady linear response of a spherical atmosphere to thermal and orographic forcing. *J. Atmos. Sci.*, **38**, 1179–1196.
- , and P. J. Valdes, 1990: On the existence of storm tracks. *J. Atmos. Sci.*, **47**, 1854–1864.
- , and F.-F. Jin, 1991: The initial value problem for tropical perturbations to a baroclinic atmosphere. *Quart. J. Roy. Meteor. Soc.*, **117**, 299–317.
- Hou, A. Y., 1993: The influence of tropical heating displacements on the extratropical climate. *J. Atmos. Sci.*, **50**, 3553–3570.
- , and R. S. Lindzen, 1992: The influence of concentrated heating on the Hadley circulation. *J. Atmos. Sci.*, **49**, 1233–1241.
- , and A. Molod, 1995: Modulation of dynamic heating in the winter extratropics associated with the cross-equatorial Hadley circulation. *J. Atmos. Sci.*, **52**, 2609–2626.
- Ioannou, P., and R. S. Lindzen, 1986: Baroclinic instability in the presence of barotropic jets. *J. Atmos. Sci.*, **43**, 2999–3014.
- Janowiak, J. E., and P. A. Arkin, 1991: Rainfall variations in the Tropics during 1986–1989, as estimated from observations of cloud-top temperatures. *J. Geophys. Res.*, **96** (Suppl.), 3359–3373.
- Lau, N. C., 1981: A diagnostic study of recurrent meteorological anomalies appearing in a 15-year simulation with a GFDL general circulation model. *Mon. Wea. Rev.*, **109**, 2287–2311.
- , 1988: Variability of the observed midlatitude storm tracks in relation to low-frequency changes in the circulation pattern. *J. Atmos. Sci.*, **45**, 2718–2743.
- Lee, W.-J., and M. Mak, 1994: Observed variability in the large-scale static stability. *J. Atmos. Sci.*, **51**, 2137–2144.
- Lindzen, R. S., 1993: Baroclinic neutrality and the tropopause. *J. Atmos. Sci.*, **50**, 1148–1151.
- , 1994: Climate dynamics and global change. *Annu. Rev. Fluid Mech.*, **26**, 353–378.
- , and A. Y. Hou, 1988: Hadley circulations for zonally averaged heating centered off the equator. *J. Atmos. Sci.*, **45**, 2416–2427.
- , and W. Pan, 1994: A note on orbital control of equator-pole heat fluxes. *Climate Dyn.*, **10**, 49–57.
- Lorenz, E. N., 1967: *The Nature and Theory of the General Circulation of the Atmosphere*. World Meteorological Organization Monogr., No. 218, 115 pp.
- Nigam, S., and R. S. Lindzen, 1989: The sensitivity of stationary waves to variations in the basic state zonal flow. *J. Atmos. Sci.*, **46**, 1746–1768.
- Oort, A. H., and J. J. Yienger, 1996: Observed long-term variability in the Hadley circulation and its connection to ENSO. *J. Climate*, **9**, 2751–2767.
- Park, C.-K., S. Schubert, D. Lamich, and Y. Kondratyeva, 1996: Monsoon rainfall in the GEOS-1 assimilation: Sensitivity to input data. NASA/GSFC Data Assimilation Office Note 96-24. [Available online at <http://dao.gsfc.nasa.gov/subpages/office-notes.html>]
- Rowntree, P. R., 1976: Response of the atmosphere to a tropical Atlantic Ocean temperature anomaly. *Quart. J. Roy. Meteor. Soc.*, **102**, 607–626.
- Sardeshmukh, P. D., and B. J. Hoskins, 1988: The generation of global rotational flow by steady idealized tropical divergence. *J. Atmos. Sci.*, **45**, 1228–1251.
- Schneider, E., 1977: Axially symmetric steady-state models of the basic state for instability and climate studies. Part II: Nonlinear calculations. *J. Atmos. Sci.*, **34**, 280–296.
- Schubert, S., C.-K. Park, C.-Y. Wu, W. Higgins, Y. Kondratyeva, A. Molod, L. Takacs, M. Seabloom, and R. Rood, 1995: A multiyear assimilation with the GEOS-1 system: Overview and results. NASA Tech. Memo. 104606, Vol. 6, NASA Goddard Space Flight Center, Greenbelt, MD, 183 pp. [Available from NASA/Goddard Space Flight Center, Greenbelt, MD 20771.]
- Simmons, A. J., J. M. Wallace, and G. W. Branstator, 1983: Barotropic wave propagation and instability, and atmospheric teleconnection patterns. *J. Atmos. Sci.*, **40**, 1363–1392.
- Takacs, L. L., A. Molod, and T. Wang, 1994: Documentation of the Goddard Earth Observing System (GEOS) General Circulation Model—Version 1. NASA Tech. Memo. 104606, Vol. 1, NASA Goddard Space Flight Center, Greenbelt, MD, 100 pp. [Available from NASA/Goddard Space Flight Center, Greenbelt, MD 20771.]
- Wallace, J. M., and D. S. Gutzler, 1981: Teleconnections in geopotential height field during the Northern Hemispheric winter. *Mon. Wea. Rev.*, **109**, 784–812.